Mitigating the atmospheric CO_2 increase and ocean acidification by adding limestone powder to upwelling regions

L. D. D. Harvey[1]
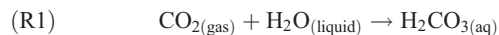
[1] The feasibility of enhancing the absorption of CO_2 from the atmosphere by adding calcium carbonate ($CaCO_3$) powder to the ocean and of partially reversing the acidification of the ocean and the decrease in calcite supersaturation resulting from the absorption of anthropogenic CO_2 is investigated. $CaCO_3$ could be added to the surface layer in regions where the depth of the boundary between supersaturated and unsaturated water is relatively shallow (250–500 m) and where the upwelling velocity is large (30–300 m a^{-1}). The $CaCO_3$ would dissolve within a few 100 m depth below the saturation horizon, and the dissolution products would enter the mixed layer within a few years to decades, facilitating further absorption of CO_2 from the atmosphere. This absorption of CO_2 would largely offset the increase in mixed layer pH and carbonate supersaturation resulting from the upwelling of dissolved limestone powder. However, if done on a large scale, the reduction in atmospheric CO_2 due to absorption of CO_2 by the ocean would reduce the amount of CO_2 that needs to be absorbed by the mixed layer, thereby allowing a larger net increase in pH and in supersaturation in the regions receiving $CaCO_3$. At the same time, the reduction in atmospheric pCO_2 would cause outgassing of CO_2 from ocean regions not subject to addition of $CaCO_3$, thereby increasing the pH and supersaturation in these regions as well. Geographically optimal application of 4 billion t of $CaCO_3$ a^{-1} (0.48 Gt C a^{-1}) could induce absorption of atmospheric CO_2 at a rate of 600 Mt CO_2 a^{-1} after 50 years, 900 Mt CO_2 a^{-1} after 100 years, and 1050 Mt CO_2 a^{-1} after 200 years.

1. Introduction

[2] The emission of CO_2 into the atmosphere from human activities leads to an increase in the partial pressure of atmospheric CO_2, and in response to this, there is a net flow of gaseous CO_2 into the surface layer of the ocean. Once dissolved in surface water, CO_2 combines with water to form a weak acid (carbonic acid, H_2CO_3), which then dissociates to bicarbonate (HCO_3^-) and carbonate (CO_3^{2-}) ions. The reactions are

(R1) $$CO_{2(gas)} + H_2O_{(liquid)} \rightarrow H_2CO_{3(aq)}$$

(R2) $$H_2CO_{3(aq)} \rightarrow H^+ + HCO_3^-$$

(R3) $$CO_3^{2-} + H^+ \rightarrow HCO_3^-,$$

giving the net reaction

(R4) $$H_2O + CO_2 + CO_3^{2-} \rightarrow 2HCO_3^- .$$

[3] Reaction (2) would tend to increase the acidity of seawater as CO_2 is added, except that CO_3^{2-} consumes the H^+ that is released by reaction (2), so that there is no change of pH as long as the occurrence of reaction (2) is balanced by reaction (3). The carbonate ion thus acts as a buffer, inhibiting changes in pH to the extent that it is available. However, the supply of CO_3^{2-} in the surface layer of the ocean is limited, so as more CO_2 is absorbed by the ocean, the H^+ concentration (and hence acidity) of ocean water increases.

[4] At the same time as ocean acidity increases, the concentration of CO_3^{2-} decreases. CO_3^{2-} is a constituent in $CaCO_3$ (calcium carbonate), which occurs in two mineral forms: aragonite, used as the structural material of corals and pteropods (high–latitude zooplankton), and calcite, used as the structural material of the foraminifera (animals ranging in size from less than 1 mm to several centimeters) and coccolithophores (a group of phytoplankton). Also, many echinoderms and mollusks and some crustaceans contain calcareous shells or exoskeletons. Although calcareous plankton account for only a few percent of marine

[1]Department of Geography, University of Toronto, Toronto, Ontario, Canada.

primary productivity [*Jin et al.*, 2006], calcareous organisms occur throughout the marine food chain, while coral reefs are thought to shelter over two million species of marine life. The surface waters of the oceans are presently supersaturated with respect to both forms of calcium carbonate, a condition that is essential for the growth and health of calcareous organisms. However, the absorption of CO_2 by the oceans reduces the degree of supersaturation by reducing the carbonate (CO_3^{2-}) concentration. Simulations reported by *Orr et al.* [2005] indicate that for a mere doubling of atmospheric CO_2 concentration (from 280 ppmv (preindustrial) to 560 ppmv), the degree of supersaturation with respect to calcite decreases from about 700% to 450% in tropical regions and from 280% to 160% in Southern Hemisphere polar regions. As for aragonite, parts of the ocean are driven to the point of being unsaturated. These decreases in the supersaturation with respect to calcite and aragonite are likely to have profoundly negative impacts on marine ecology and productivity [*Riebesell et al.*, 2000; *Orr et al.*, 2005; *Raven et al.*, 2005; *Ruttimann*, 2006; *Gazeau et al.*, 2007] and imply that a "safe" atmospheric CO_2 concentration is well below a doubling of the preindustrial concentration. In as much as the current CO_2 concentration has already risen from 280 ppmv to 380 ppmv and is unlikely to be stabilized at less than 450 ppmv even with extreme efforts to reduce emissions, it is clear that significant negative oceanic ecological impacts are now unavoidable unless some mitigation not previously considered can be undertaken.

[5] The carbonate concentration required for supersaturation increases with increasing pressure and hence with increasing depth in the ocean. As a result, deep ocean waters are unsaturated with respect to $CaCO_3$, and carbonate sediments produced by the downward rain of dead calcareous plankton accumulate only on the shallower ocean floor (above depths ranging from about 0.3 km to 4 km). Over a period of several thousand years, the decrease in CO_3^{2-} concentration as the ocean absorbs anthropogenic CO_2 will induce the dissolution of the deepest carbonate sediments, as water that had been supersaturated becomes unsaturated. This will restore the CO_3^{2-} that had been depleted from ocean water, neutralize the increase in acidity of ocean water, and allow the ocean to absorb further CO_2 from the atmosphere over a period of several thousand years.

[6] The whole process can be sped up if finely ground limestone, which is overwhelmingly $CaCO_3$, were to be sprinkled into the surface layer of the ocean and allowed to sink into unsaturated deep water, where it would dissolve. The reaction when $CaCO_3$ dissolves is

$$(R5) \qquad CaCO_3 \rightarrow Ca^{2+} + CO_3^{2-} .$$

[7] This induces reaction (3) to occur, which reduces the acidity, but to the extent that reaction (3) is followed by reactions (2) and (1), the net result is reaction (4) plus reaction (5), giving

$$(R6) \qquad CaCO_3 + CO_2 + H_2O \rightarrow Ca^{2+} + 2HCO_3^- .$$
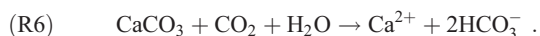
[8] According to reaction (6), the dissolution of one mole of $CaCO_3$ is accompanied by the uptake of one mole of CO_2

and no net change in acidity. As will be seen below, reaction (5) is not fully accompanied by reaction (4), so less than one mole of CO_2 is taken up per mole of $CaCO_3$ dissolved, and there is a net reduction in acidity. Similar reactions occur involving $MgCO_3$ (a component of dolomite, $CaMg(CO_3)_2$). Finely ground limestone could be sprinkled over the ocean using a flotilla of ships crisscrossing the most promising regions of the ocean. If this were done in regions where the saturation horizon is shallow and where strong upwelling (>50 m a^{-1}) occurs (the two conditions tend to be correlated with one another), water with restored CO_3^{2-} could be available to absorb more atmospheric CO_2 within as little as a few years after the addition of $CaCO_3$.

[9] The purposes of this paper are (1) to estimate the areal extent of the ocean with conditions suitable for the rapid absorption of anthropogenic CO_2 through the addition of limestone powder, (2) to estimate the maximum rate at which CO_2 could be absorbed from the atmosphere and the associated effectiveness of limestone addition (in terms of the ratio of mass of CO_2 absorbed to mass of limestone added), and (3) to assess the potential impact of limestone addition on the atmospheric CO_2 concentration and on the pH and degree of supersaturation of surface waters, both in the regions where limestone is added and globally. Global data sets of oceanographic chemical properties and upwelling velocity are used to identify promising regions of the ocean. A simple model of the dissolution of falling $CaCO_3$ particles is used in a 1-D advection-diffusion model of an ocean column with explicit carbonate chemistry to assess the release and vertical transport of dissolved limestone. The column model is applied at all grid points on a $1° \times 1°$ horizontal grid that had been identified as promising regions for addition of limestone powder and is used to assess the potential rate of absorption of atmospheric CO_2, in the absence of feedback on atmospheric CO_2 concentration. Results from these simulations are used along with the results of a perturbation analysis to guide the choice of parameters in simulations using a global low-resolution upwelling diffusion climate-carbon cycle model, in which the rate of the limestone dissolution flux is directly prescribed. This model allows for feedback between enhanced oceanographic uptake of atmospheric CO_2 and atmospheric CO_2 concentration and is used to assess the net effect on peak and century timescale atmospheric CO_2 and ocean pH of scenarios involving various combinations of stringent reductions in fossil fuel use, adding limestone powder, and sequestration of CO_2 from bioenergy.
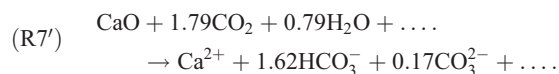
[10] The central idea of this paper (to enhance oceanic uptake of anthropogenic CO_2 by direct addition of limestone powder to the ocean surface) was inspired by the earlier work of *Rau and Caldeira* [1999], *Caldeira and Rau* [2000], and *Rau et al.* [2007]. They suggested reacting captured fossil fuel CO_2 with limestone in reaction chambers on land before releasing it into the ocean, rather than directly injecting captured CO_2 into the deep ocean, as in the conventional ocean carbon sequestration concept [*Intergovernmental Panel on Climate Change (IPCC)*, 2005]. Their scheme avoids the impacts on ocean acidity and the eventual outgassing of about 15% of the injected CO_2 that would occur with conventional oceanic carbon sequestration but would require a large infrastructure to mine, crush, and transport a mass of limestone several

times the mass of captured CO_2, as well as an infrastructure to pump seawater and captured CO_2 to the dissolution sites and to pipe the reaction mixture to the ocean over a sufficiently dispersed area. The idea proposed here is somewhat simpler, in that the crushed limestone would be directly sprinkled over the ocean surface, without the need to build reaction chambers on land, pump seawater to the chambers, and then pump the reaction products out to sea. Furthermore, the effectiveness in terms of moles of CO_2 absorbed per mole of $CaCO_3$ that needs to be mined (about 0.7 in the scheme proposed here if all of the dissolved $CaCO_3$ eventually returns to the surface layer) would be significantly larger than the CO_2 emission that would be avoided if captured CO_2 is reacted with $CaCO_3$ prior to injection into the ocean (the avoided emission in that case is the outgassing that would occur if captured CO_2 were directly injected into the deep ocean; this avoided outgassing is about 0.15 moles of CO_2 for every mole of $CaCO_3$ that is used, and it would occur several hundred years after injection). Fossil fuel CO_2 could still be captured but would be sequestered in the more limited geological reservoirs available on land.

[11] *Kheshgi* [1995] suggested enhancing the absorption of CO_2 by the oceans by adding the dissolution products of alkaline minerals to the ocean. He notes that soda ash (Na_2CO_3) is readily soluble in surface seawater but is limited in supply (sufficient to offset only 6 Gt C if the entire world reserve were dissolved into the ocean). To overcome the problem that $CaCO_3$ is not soluble in ocean surface water, *Kheshgi* [1995] explored the option of producing lime through the reaction

(R7) $CaCO_3 + 178 kJ/mole \rightarrow CaO + CO_2,$
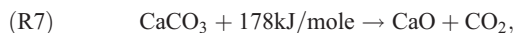
followed by dissolution of CaO in the ocean, which involves the reaction

(R7′) $\begin{aligned} &CaO + 1.79 CO_2 + 0.79 H_2O + \ldots. \\ &\quad \rightarrow Ca^{2+} + 1.62 HCO_3^- + 0.17 CO_3^{2-} + \ldots. \end{aligned}$

[12] The net result is the removal of 0.79 moles of CO_2 for every mole of $CaCO_3$ used, which would be reduced to 0.38 moles if coal is used to produce the heat needed by the reaction. The net removal of CO_2 would be greater if the CO_2 produced by reaction (7) and the CO_2 released by combustion were captured in part and buried in the same way that capture and sequestration of CO_2 from power plants has been considered.

2. Estimation of the Suitable Ocean Area

[13] The GLODAT 3-D data set (GLODAT 3-D data are available at http://cdiac.esd.ornl.gov/oceans/home.html and described by *Key et al.* [2004]) of ocean total dissolved inorganic carbon (TDIC) (the sum of dissolved CO_2, CO_3^{2-}, and HCO_3^-), total alkalinity (TALK), and phosphate was used to compute the 3-D CO_3^{2-} concentration field. These data are available on a on a $1° \times 1°$ latitude-longitude grid and at 33 different depths. Mean annual temperature and salinity data (needed for this calculation) on the same grid as the TDIC, alkalinity, and phosphate data were obtained from the NODC/NOAA World Ocean Atlas (NODC/NOAA

World Ocean Atlas data are available at http://ingrid.ldeo. columbia.edu/SOURCES/.NOAA/.NODC/.WOA01). Limestone consists overwhelmingly of calcite, so the degree of supersaturation or undersaturation with respect to calcite and the variation in the depth of the boundary between these two zones (subsequently referred to as the "saturation depth") is of interest here. The CO_3^{2-} concentration field was calculated using the algorithm given in the appendix to the work by *Peng et al.* [1987] for the solution of the carbonate chemistry equations, except that the carbonic acid dissociation constants of *Dickson and Millero* [1987] and the boric acid dissociation constant of *Dickson* [1990] were used in place of those given by *Peng et al.* [1987], with all reaction constants converted to a common pH scale. The use of these constants results in a computed global mean mixed layer pCO_2 of 338 ppmv, which is rather low given that the GLODAT data correspond to about 1995, when atmospheric CO_2 was at 360 ppmv. The low global mean mixed layer pCO_2 is likely due to a summer bias in the GLODAT surface data; according to *Takahashi et al.* [2008], summer mixed layer pCO_2 is 20–30 ppmv lower than the annual mean at high latitudes in both hemispheres. In any case, this offset will have no effect on the results presented here, which involve perturbation fluxes.

[14] The CO_3^{2-} concentration required for saturation ($[CO_3^{2-}]_{sat}$) with respect to calcite is computed as by *Broecker and Takahashi* [1978], namely,

$$[CO_3^{2-}]_{sat} (\mu mole\ kg^{-1}) = 47.5 e^{z/6250}, \qquad (1)$$

where z is the depth in m. The $[CO_3^{2-}]_{sat}$ required for saturation depends on the $[Ca^{2+}]$, which is fixed for a given ocean salinity. Equation (1) pertains to a salinity of 35‰, and the very small spatial variation in oceanic salinity is neglected here.

[15] The geographical variation in the depth of the boundary between supersaturated and unsaturated water with respect to calcite is shown in Figure 1 (top). The saturation depth is in excess of 4000 m in the North Atlantic Ocean and progressively decreases in the direction of deep water flow (because of the cumulative impact of the rain and dissolution of organic matter from the surface layer, which releases CO_2 that in turn reduces the CO_3^{2-} concentration through reaction (4)). In much of the North Pacific Ocean, the saturation depth is less than 500 m deep, and along parts of the west coast of North and South America, it is less than 250 m deep.

[16] Upwelling velocities throughout the world ocean have been estimated by *Wunsch and Heimbach* [2000] using inverse calculation techniques, which are inherently sensitive to small errors in the input data. The resulting calculated velocity field is only indicative of the real field. Here the velocity fields on a $1° \times 1°$ latitude-longitude grid at various depths and averaged over the period January 1992 to January 2005 (available at http://batsi.mit.edu:8080/ las/servlets/dataset?catitem=2) have themselves been vertically averaged to produce a single indicative upwelling velocity at each horizontal grid point. Vertical averaging was performed over a depth interval ranging from a depth of 185 m to 1000 m below the initial depth of the saturation horizon in each column, as all of the added limestone
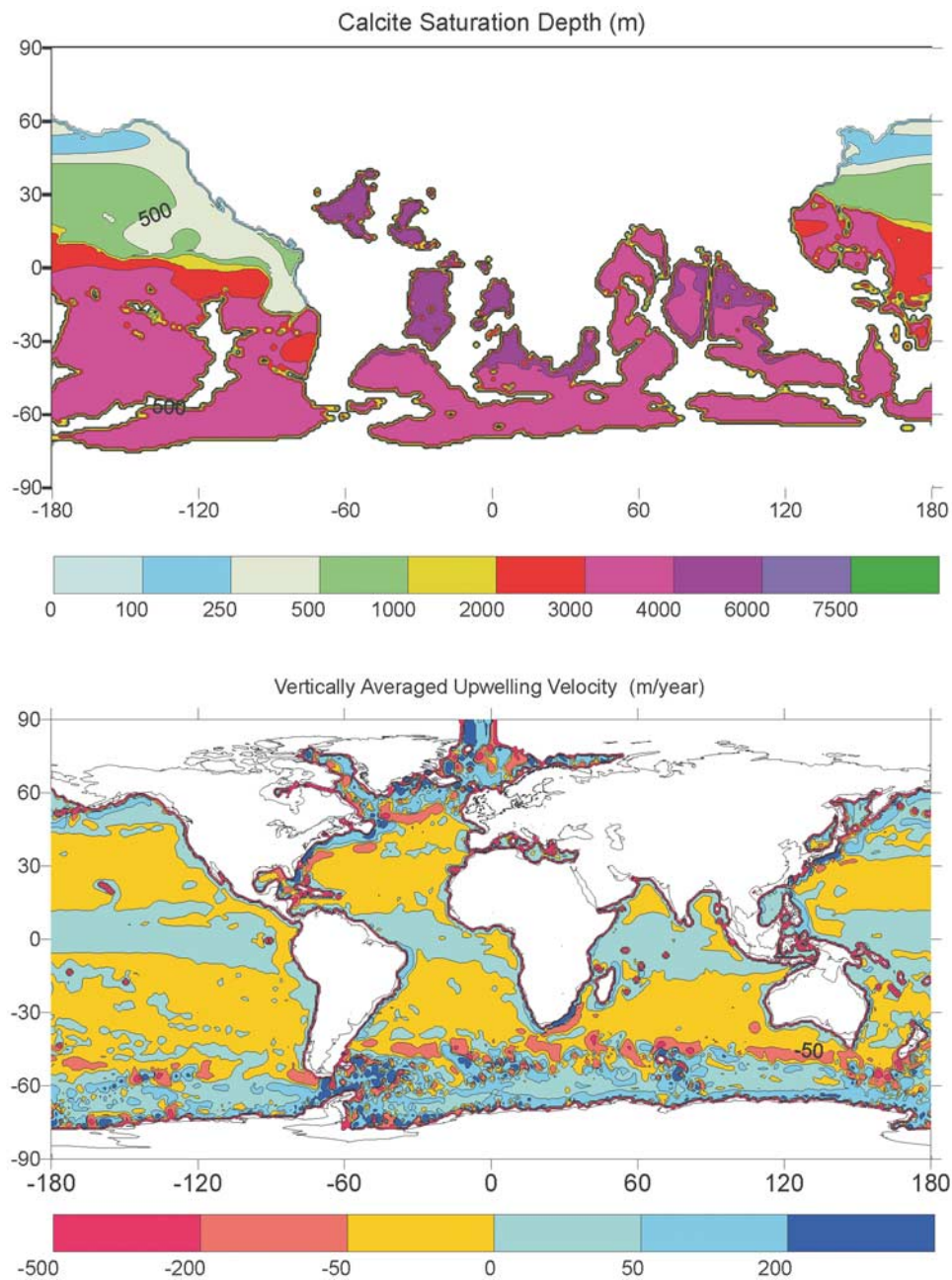
Figure 1. (top) The depth of the boundary between saturated and unsaturated waters for calcite, as computed using the algorithm for solving the carbonate chemistry equations given by *Peng et al.* [1987] and using the GLODAP and NOAA ocean data sets as inputs. (bottom) Upwelling velocity (m a^{-1}) average between a depth of 185 m and a depth 1000 m below the saturation boundary, computed from the data set described by *Wunsch and Heimbach* [2000]. Negative values denote downwelling.

powder dissolves within 1000 m of the saturation horizon. Figure 1 (bottom) shows the resulting upwelling velocity field. Upwelling tends to occur in regions where it would be expected, on the basis of the well-known pattern of wind-induced Ekman currents in the ocean mixed layer, including in much of the North Pacific Ocean where the saturation depth is 500 m or less. The saturation depth divided by the mean upwelling velocity provides an estimate of the time required for water from the saturation depth to reach the ocean surface. The ocean areas with upwelling times in the

first 20 bins of 5 years' width are given in Table 1. The ocean areas with upwelling times of 25, 50, or 100 years or less are about 9, 16, and 28 million km^2, respectively, or about 2.5, 4.5, and 8.0% of the global ocean area of 356 million km^2.

3. Simulation of the Effect of Limestone Addition

[17] A model of the downward settling of limestone powder, its dissolution, and the subsequent upwelling of

Table 1. Ocean Area Where the Time Required for Water to Upwell from the Calcite Saturation Horizon to the Surface Falls Within the Indicated Time Intervals[a]

Upwelling Time, years	Ocean Area, Million km²		Number of 1° × 1° Grid Cells
	By Bin	Cumulative	
0−5	2.58	2.58	331
5−10	2.22	4.80	287
10−15	1.33	6.14	170
15−20	1.49	7.63	193
20−25	1.59	9.22	216
25−30	1.33	10.55	177
30−35	1.36	11.91	181
35−40	1.35	13.26	178
40−45	1.34	14.60	181
45−50	1.46	16.06	188
50−55	1.67	17.73	210
55−60	1.39	19.12	184
60−65	1.43	20.55	182
65−70	1.46	22.01	181
70−75	1.42	23.43	179
75−80	1.04	24.47	138
80−85	1.06	25.53	149
85−90	0.91	26.44	127
90−95	0.97	27.41	130
95−100	0.98	28.39	131

[a]By comparison, the global ocean area is about 356 million km². A total of 3713 grid cells are involved in upwelling times of up to 100 years.

dissolution products is presented below, followed by sensitivity tests on five representative columns, then results from the simulation of all the columns included in all the bins given in Table 1.

3.1. Description of the Column Model

[18] Limestone is assumed to be ground to particles of radius r, which have a fall velocity given by Stoke's law as

$$V = \frac{2}{9} g \left(\frac{\rho_p - \rho_w}{\eta} \right) r^2, \qquad (2)$$

where ρ_p and ρ_w are the particle and water densities, respectively (equal to 2800 and 1027 kg m^{-3}, respectively), and η is the viscosity of water (equal to 8.9×10^{-4} Pa s). For an initial radius of 40 μm, the initial fall velocity is 609 m d^{-1}. The dissolution rate (expressed as the rate of decrease in the particle radius) is computed as

$$D = \left\{ \begin{array}{l} C_{dis}(C_{sat} - C_{amb}), C_{amb} < C_{sat} \\ 0, \underline{\qquad\qquad} C_{amb} > C_{sat} \end{array} \right\}, \qquad (3)$$

where C_{dis} is a constant with units of m s^{-1} μmole^{-1} kg^{-1}, and C_{amb} and C_{sat} are the ambient and saturation CO_3^{2-} concentrations. This is consistent with first-order kinetics, which is a widely used parameterization of carbonate dissolution kinetics [Hales and Emerson, 1997; Morse and Arvidson, 2002]. The vertical profile of the dissolution of a single falling particle is computed five times per year using time steps of 31,536 s (1/1000th of a year). The vertical column is divided into 500 layers of equal thickness (typically 2−4 m thick, depending on the depth of the column). The dissolution flux into each model layer from a single particle is computed on basis of the change in particle volume as it passes through each layer and multiplied by the total number of particles associated with a given annual rate of application of $CaCO_3$. This gives the annual flux of alkalinity and TDIC into each model layer. These source terms are used in an advection-diffusion equation that is integrated using time steps of 1/100th of a year. This is an asynchronous integration procedure, in that shorter time steps are used to simulate the dissolution profile of a falling particle, which changes only slowly as the ambient conditions change, then the latest dissolution profile is used in longer time steps to update the ambient conditions for 20 time steps before the dissolution profile is recomputed. The dissolution of $CaCO_3$ increases both $[CO_3^{2-}]_{sat}$ and $[Ca^{2+}]$, but the relative impact on $[Ca^{2+}]$ is negligible compared to the effect on $[CO_3^{2-}]_{sat}$ because of the fact that (1) a typical initial $[CO_3^{2-}]_{sat}$ is 160 μmole kg^{-1} while $[Ca^{2+}]$ = 10,300 μmole kg^{-1} at a salinity of 35‰, and (2) usually not more than about 40 μmole kg^{-1} of dissolved $CaCO_3$ is added at any depth. Thus changes in $[Ca^{2+}]$ can be ignored.

[19] Any remaining $CaCO_3$ particles that reach the sea floor are assumed to accumulate without further dissolution. Undissolved particles may reach the seafloor if, as sometimes happens, the initial application and dissolution of $CaCO_3$ drives the previously unsaturated deep water to a saturated or nearly saturated state.

[20] Over time, carbonate-enriched subsurface water upwells to the surface (mixed) layer, leading to steady state increases in the mixed layer alkalinity and TDIC ($\Delta TDIC_p$). The resulting reduction in mixed layer pCO_2 is computed using the carbonate chemistry equations of Peng et al. [1987] but with the carbonic acid and boric acid dissociation constants of Dickson and Millero [1987] and Dickson [1990], respectively. In response to reduced mixed layer pCO_2, there will be a perturbation flow of CO_2 into the mixed layer (superimposed on the local background flow, which could be into or out of the mixed layer), increasing the mixed layer pCO_2 until the original pCO_2 is exactly restored (neglecting, for the moment, the decrease in atmospheric pCO_2 resulting from the CO_2 flux into the ocean). The increase in TDIC in the mixed layer required to restore the original mixed layer pCO_2, $\Delta TDIC_a$, is computed here using a Newton-Raphson iteration. The time constant for equilibration of mixed layer pCO_2 with the atmosphere is equal to the average residence time of CO_2 in the mixed layer (about 7 years) divided by the buffer factor (about 10), and so is less than 1 year [see Harvey, 2000, chapter 8]. This is short enough that the mixed layer pCO_2 and TDIC will have time to largely or fully adjust to the added carbonate.

[21] One can thus envisage the process as a conveyor belt of carbonate-enriched subsurface water that rises to the surface, absorbs CO_2 from the atmosphere, and then spreads horizontally to regions that may or may not have also received limestone powder. The absorbed CO_2 and alkalinity perturbation will eventually diffuse into the thermocline away from upwelling regions. The total absorption of CO_2 will thus be related to the amount of dissolved $CaCO_3$ that has been advected into and passed through the mixed layer, which can be computed as the cumulative addition of $CaCO_3$ to the column minus the amount in the column below the base of the mixed layer and minus any cumulative burial of undissolved $CaCO_3$. For columns with a
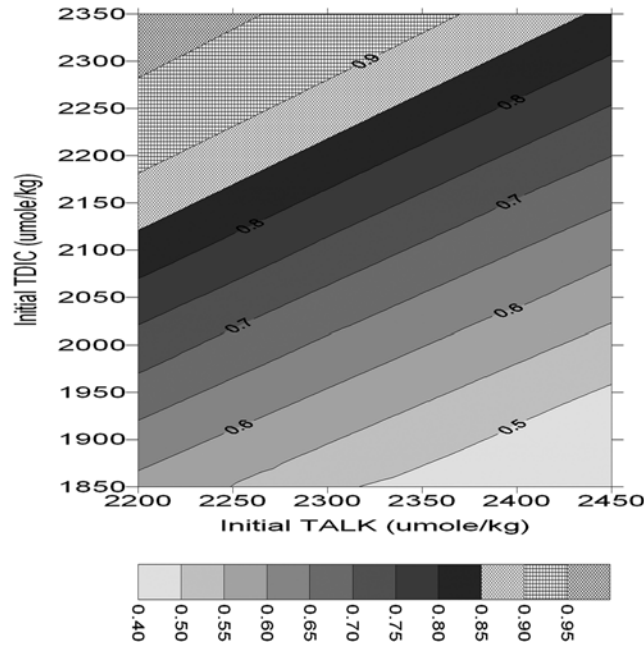
Figure 2. The molar ratio (moles of CO_2 absorbed from the atmosphere over moles of dissolved $CaCO_3$ added to the mixed layer) for a perturbation in TDIC of 10 μmole kg^{-1} due to dissolution of $CaCO_3$, as a function of the initial TDIC and TALK.

shallow saturation depth and strong upwelling, the amount of $CaCO_3$ products in the mixed layer as a fraction of the added $CaCO_3$ asymptotes to 1.0 over time; that is, essentially all of the added $CaCO_3$ participates in absorption of atmospheric CO_2. If F is the fraction of added $CaCO_3$ that passes through the mixed layer in dissolved form, then the ratio R of mass of CO_2 absorbed from the atmosphere to mass of $CaCO_3$ added is given by

$$R = F\left(\frac{\Delta\mathrm{TDIC}_a}{\Delta\mathrm{TDIC}_p}\right)\left(\frac{\mathrm{MW_{CO2}}}{\mathrm{MW_{CaCO3}}}\right), \quad (4)$$

where $\mathrm{MW_{CO2}}$ and $\mathrm{MW_{CaCO3}}$ are the molecular weights of CO_2 and $CaCO_3$ (44 and 100 gm mole^{-1}, respectively). The ratio $\Delta\mathrm{TDIC}_a/\Delta\mathrm{TDIC}_p$ is the ratio of moles of CO_2 absorbed to moles of dissolved $CaCO_3$ added to the water volume that exchanges CO_2 with the atmosphere. R times the cumulative addition of $CaCO_3$ gives the cumulative absorption of CO_2 from the atmosphere. Alternatively, the absorption A_{year} (kg m^{-2} a^{-1}) in any given year can be computed as

$$A_{\mathrm{year}} = \Delta\mathrm{TDIC}_a \rho_w w \mathrm{MW_{CO2}} \times 10^{-9}, \quad (5)$$

where w is the upwelling velocity in m a^{-1}. The cumulative absorption of CO_2 computed by summing the annual values given by equation (5) agrees to within 1% with the estimate based on equation (4).

[22] Given that the change in mixed layer pCO_2 after adjustment of the mixed layer to the addition of dissolved $CaCO_3$ is zero, one can write

$$\Delta\mathrm{TDIC}_a \frac{\partial p\mathrm{CO}_2}{\partial \mathrm{TDIC}} + \Delta\mathrm{TDIC}_p \frac{dp\mathrm{CO}_2}{d\mathrm{TDIC}} = 0, \quad (6)$$

where $\partial pCO_2/\partial\mathrm{TDIC}$ is the rate of change in pCO_2 when TDIC alone is changed, while $dpCO_2/d\mathrm{TDIC}$ is the rate of change of pCO_2 when TDIC changes because of addition of $CaCO_3$, which also changes TALK. For small perturbations, $dpCO_2/d\mathrm{TDIC}$ is given by

$$\frac{dp\mathrm{CO}_2}{d\mathrm{TDIC}} = \frac{\partial p\mathrm{CO}_2}{\partial\mathrm{TDIC}} + \frac{\partial p\mathrm{CO}_2}{\partial\mathrm{TALK}}\frac{d\mathrm{TALK}}{d\mathrm{TDIC}} = \frac{\partial p\mathrm{CO}_2}{\partial\mathrm{TDIC}} + 2\frac{\partial p\mathrm{CO}_2}{\partial\mathrm{TALK}} < 0. \quad (7)$$

From equation (6), it follows that the molar ratio M_R is given by

$$M_R = \frac{\Delta\mathrm{TDIC}_a}{\Delta\mathrm{TDIC}_p} = -\frac{dp\mathrm{CO}_2/d\mathrm{TDIC}}{\partial p\mathrm{CO}_2/\partial\mathrm{TDIC}}. \quad (8)$$

[23] Both the partial and total derivatives vary strongly with the initial TALK, TDIC, temperature and for perturbations larger than 10 μmole kg^{-1}, with the magnitude of the perturbation. However, the ratio of the two derivatives (which gives the molar ratio) is much less sensitive to these conditions. This is shown in Figure 2, which gives M_R as a function of the initial TALK and TDIC of a water parcel, as computed by solving the carbonate chemistry equations. Points corresponding to the columns with upwelling times of 100 years or less correspond largely to the bottom left quadrant of Figure 2 (specifically, TALK varies from 2200 μmole kg^{-1} to 2325 μmole kg^{-1}, and TDIC varies from 1900 μmole kg^{-1} to 2200 μmole kg^{-1}). M_R is typically between 0.6 and 0.8 for the chosen columns. M_R is shown in Figure 2 for $\Delta\mathrm{TDIC}_p = 10$ μmole kg^{-1} but is almost identical for $\Delta\mathrm{TDIC}_p = 1-100$ μmole kg^{-1}. Thus increasing the rate at which $CaCO_3$ is applied may decrease F (as the saturation horizon and dissolution profile are shifted to greater depths when $CaCO_3$ is added at a greater rate), but it will have negligible effect on the molar ratio.

3.2. Results of Sample Simulations With the Column Model

[24] As an initial exploration of the effectiveness of adding finely ground limestone at the ocean surface, simulations were performed for five columns, which are listed in Table 2 along with relevant data. Table 3 gives the steady state $\Delta\mathrm{TDIC}_p$, ΔpCO_2, $\Delta\mathrm{TDIC}_a$, the molar ratio $\Delta\mathrm{TDIC}_a/\Delta\mathrm{TDIC}_p$, the efficiency of $CaCO_3$ utilization F, and the absorption mass ratio R after 200 years of applying $CaCO_3$ at a rate of 200 gm m^{-2} a^{-1}. In most cases, the steady state changes are established within a few years to decades after application of limestone powder begins. The molar ratios are consistent with the values expected from equation (8). The fraction F depends strongly on the initial conditions in the column and whether or not the addition of $CaCO_3$ powder drives parts of the columns from an unsaturated to supersaturated state. Figure 3 shows the initial vertical profile of the saturation ratio for calcite for the five columns. Except for the first column, addition of $CaCO_3$ at a rate of 200 gm m^{-2} a^{-1} and its subsequent dissolution drives part of the column to a saturated state, such that some of the applied $CaCO_3$ reaches the ocean floor (and is assumed here not to dissolve). R is about 0.3 for the first column but only 0.014 for the fifth column, as all except the

Table 2. The Ocean Columns Analyzed Here[a]

	Location		Initial Surface Conditions					
Column	Longitude	Latitude	TALK, μmole kg^{-1}	TDIC, μmole kg^{-1}	T, °C	pCO$_2$, μatm	Upwelling Velocity, m a^{-1}	Initial Saturation Depth, m
1	175°W	54°N	2219.1	2015.8	5.5	273.8	50.3	219
2	150°E	53°N	2215.0	1981.7	4.0	214.0	28.9	204
3	136°W	50°N	2207.7	1996.4	10.2	309.2	29.0	334
4	161°E	35°N	2265.8	1951.5	20.0	295.6	36.8	749
5	124°E	16°N	2253.7	1944.3	28.4	419.6	28.1	2804

[a]TDIC, total dissolved inorganic carbon; T, temperature.

lowest 100 m of this column become supersaturated, and R is in between for the other columns.

[25] Also given in Table 3 are the initial changes in mixed layer pH and percent supersaturation due to the addition of dissolved CaCO$_3$, the adjustment in pH and supersaturation due to the absorption of CO$_2$ from the atmosphere, and the final changes in pH and supersaturation. The adjustment offsets about 75–80% of the initial increase in pH and about 55–65% of the increase in supersaturation.

[26] These results are for an initial particle radius of 40 μm and for C$_{dis}$ = 1 × 10^{-10} m s^{-1}. Figure 4 compares the cumulative absorption of CO$_2$ after 200 years for each column for the cases with initial particle radii of 10 and 40 μm and for C$_{dis}$ = 1 × 10^{-10} and 1 × 10^{-11} m s^{-1}. The appropriate value of the dissolution coefficient is uncertain (in part because it depends on the details of the particle shape and on surface irregularities) but is likely to fall within this range, as this range results in dissolution occurring within a few 100 m to 1 km of the saturation horizon, which matches observations of the distribution of CaCO$_3$ in ocean sediments. Fortunately, the cumulative absorption of CO$_2$ is remarkably insensitive to a factor of 10 variation in the dissolution coefficient. Grinding the CaCO$_3$ to 10-μm particles increases the mass absorption ratio by 5% or less for columns where F is substantially less than 1 because in this case, more of the particles are dissolved before reaching

the sea floor (at which point no further dissolution is assumed to occur). For the first column, where F = 0.943, grinding the CaCO$_3$ to 10 μm has a negligible effect on the absorption of CO$_2$. As there is an energy penalty (as discussed in section 5.2) in grinding CaCO$_3$ to a smaller size, optimization will require grinding the CaCO$_3$ to different sizes, depending on the location where it will be applied.

[27] As long as the underlying column is not driven to a saturated state, the absorptive capacity in a given region is not likely to decrease over time. This is because, even if the downwelled water eventually recirculates back to the columns where CaCO$_3$ is being added, its CO$_3^{2-}$ concentration will have been depleted by the absorption of CO$_2$ from the atmosphere during its transit through the mixed layer. Thus the process can continue indefinitely. However, one could achieve a gradual increase in the rate of absorption if, at the same time the addition of CaCO$_3$ begins in the quick response regions, CaCO$_3$ is also added to regions with a deeper saturation horizon and/or smaller upwelling velocity. Absorption of atmospheric CO$_2$ from these regions will be delayed relative to absorption from the high-priority regions, and, as well, a smaller fraction of the added CaCO$_3$ would be advected into the mixed layer. However, much larger eventual rates of CO$_2$ absorption can be achieved in this way.

Table 3. Steady State Impact on Mixed Layer Properties of Applying 200 gm m^{-2} a^{-1} of CaCO$_3$ (Assumed to be Calcite) at 40 μm Radius With C$_{dis}$ = 10^{-10} m s^{-1} μmole^{-1} kg^{-1}

	Changes Prior to Absorption of Atmospheric CO$_2$ (Changes in TALK Are Twice Those of TDIC)		Equilibrium Adjustment of TDIC, μmole kg^{-1}	Moles CO$_2$ Absorbed Over Moles CaCO$_3$ Added	Fraction of Added CaCO$_3$ in the Mixed Layer (F)	Mass of CO$_2$ Absorbed Over Mass of CaCO$_3$ Added (R)
Column	TDIC, μmole kg^{-1}	pCO$_2$, μatm				
1	39.8	−40.5	28.9	0.727	0.943	0.302
2	37.6	−27.5	26.2	0.696	0.501	0.153
3	44.4	−48.7	31.7	0.714	0.587	0.184
4	33.4	−26.7	20.5	0.613	0.522	0.141
5	8.5	−10.3	5.2	0.615	0.052	0.014

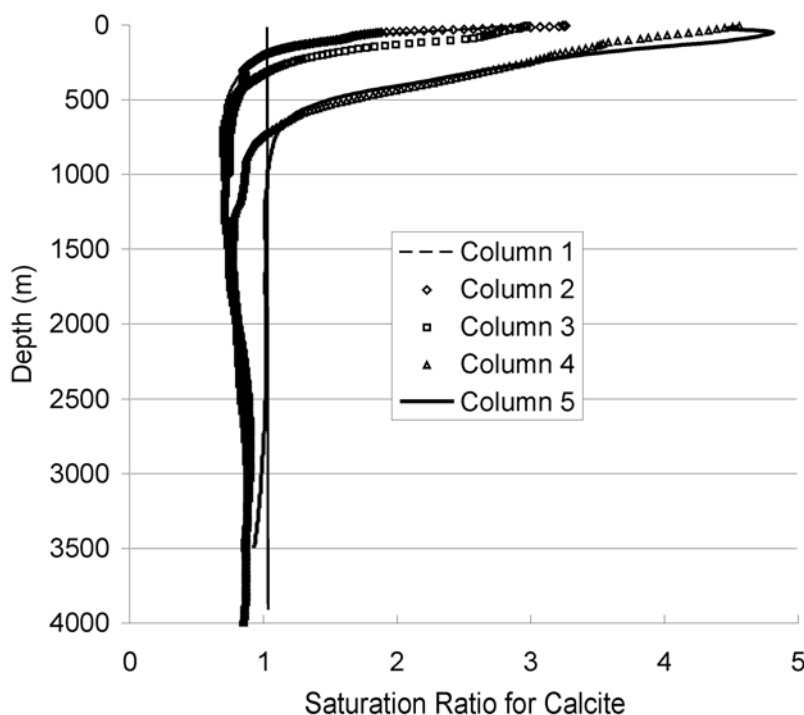|	Changes in pH			Changes in Supersaturation		
Column	Initial	Adjustment	Final	Initial, %	Adjustment, %	Final, %
1	0.073	−0.059	0.014	55	−36	19
2	0.063	−0.050	0.013	63	−34	20
3	0.078	−0.063	0.015	62	−41	22
4	0.044	−0.033	0.011	51	−28	23
5	0.012	−0.009	0.003	13	−7	6

Figure 3. Vertical profile of saturation ratio for calcite for the five columns listed in Table 2.

[28] The results presented here may be somewhat optimistic, in that all of the water upwelling from depth is assumed to enter the mixed layer, whereas in reality, there could be some detrainment of upwelling water below the mixed layer. This would cause the F computed here to be too large. On the other hand, the volume of water and hence the fraction of added limestone interacting with the atmosphere will be governed by the winter mixed layer depth, which reaches several hundred m at high latitudes. Thus application of limestone powder to the oceans may be most effective if applied to high-latitude regions with a shallow saturation depth and strong upwelling velocity.

3.3. Simulations With All Eligible Columns

[29] The column model was used to estimate the rate of absorption of CO_2 from the atmosphere when crushed
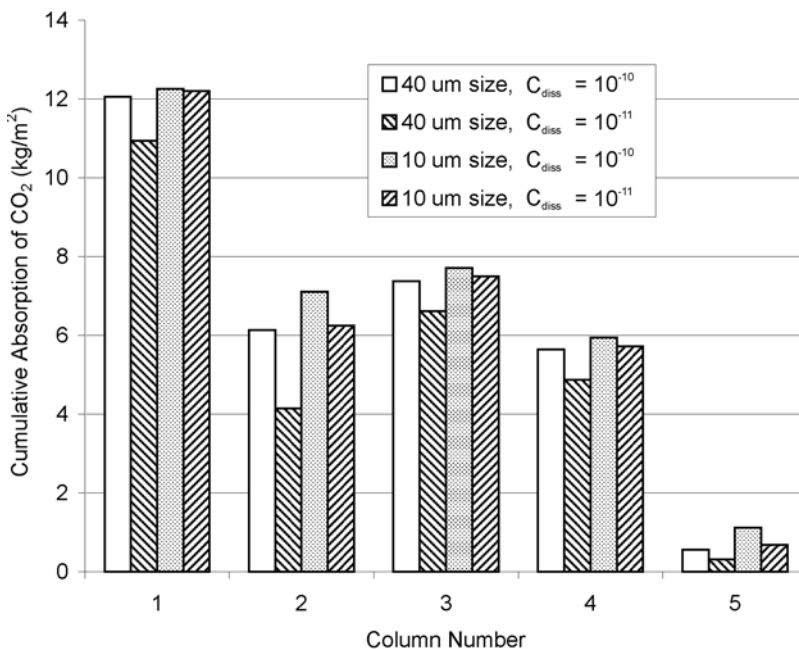

Figure 4. Impact of alternative initial particle radii and dissolution coefficients on the cumulative absorption of CO_2 after 200 years when limestone powder is added at a rate of 200 gm m^{-2} a^{-1}.
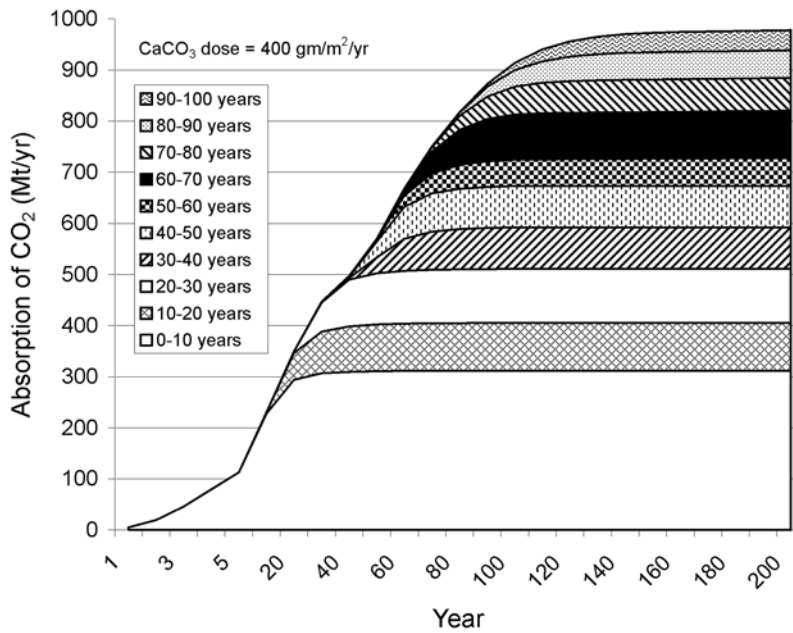
Figure 5. Rate of absorption of atmospheric CO_2 resulting from applying $CaCO_3$ powder at a rate of 400 gm m^{-2} a^{-1} grouped according to columns in 10-year upwelling time bins.

$CaCO_3$ is assumed to be applied to all 3713 $1° \times 1°$ grid cells with upwelling times of 100 years or less. The simulations were carried out for 200 years. Figure 5 shows the variation in the rate of absorption of CO_2 broken down into contributions from columns with upwelling times of 0–10 years, 10–20 years, and so on, when 80-μm diameter $CaCO_3$ powder is applied everywhere at a rate of 400 gm m^{-2} a^{-1}. The rate of absorption reaches 900 Mt after 100 years and 970 Mt after 200 years. However, applying $CaCO_3$ at a spatially uniform rate is not the most effective procedure because the absorption rate is saturated for some columns long before the application rate reaches 400 gm m^{-2} a^{-1}, whereas for other columns, the absorption rate is still rather responsive to an increasing application rate. This is illustrated in Figure 6, which computes the average effectiveness of $CaCO_3$ addition (annual rate of absorption
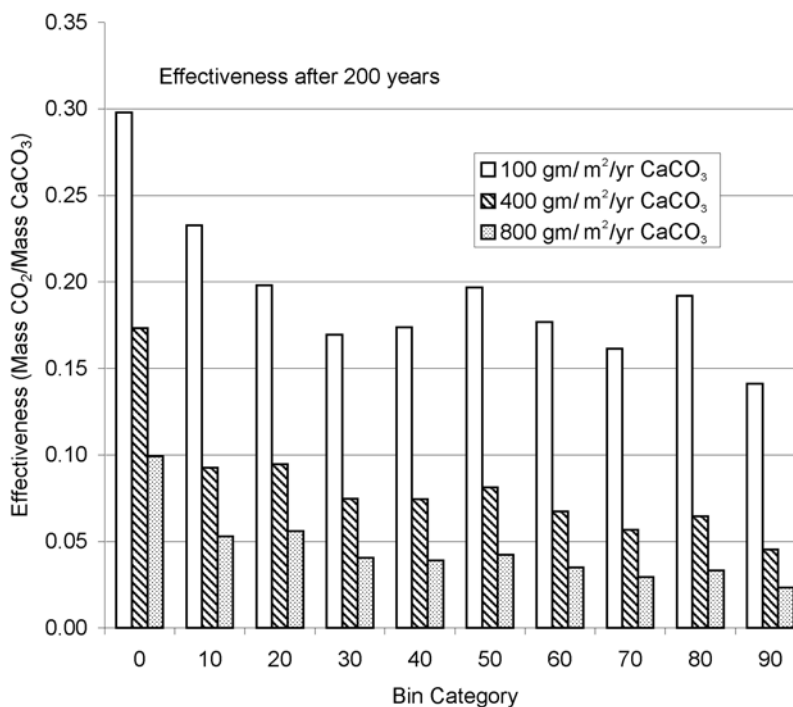

Figure 6. Average effectiveness of columns in different upwelling time bins for three different rates of application of $CaCO_3$.
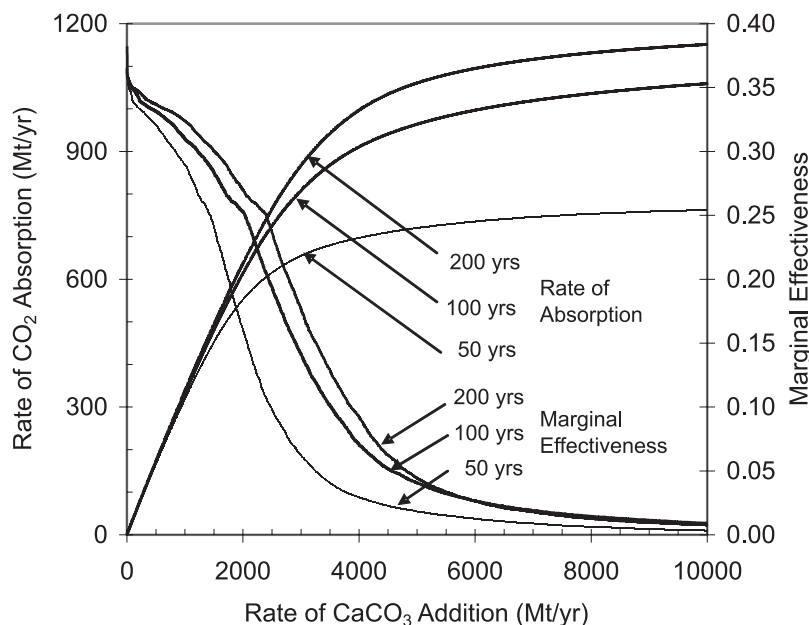
Figure 7. Rate of absorption of atmospheric CO_2 as the rate of addition of $CaCO_3$ increases, beginning with the most effective column/dose increment combination and working to progressively less effective combinations.

of CO_2 divided by annual rate of addition of $CaCO_3$) averaged over all the columns in 10-year bins, for application rates of 100, 400, and 800 gm m^{-2} a^{-1}. The largest bin-averaged effectiveness is about 0.30, which results from the CO_2:$CaCO_3$ molecular weight ratio (0.44) times a molar ratio of about 0.7 with F (in equation (4)) equal to about 1.0. After 100 years, columns in bins with a short upwelling time tend to be more effective at an application rate of 800 gm m^{-2} a^{-1} than columns in the bins with the longest upwelling times and an application rate of only 100 gm m^{-2} a^{-1}. After 200 years, the reverse is true.

[30] In order to determine the spatial distribution of $CaCO_3$ additions that minimizes the total amount of $CaCO_3$ added for a given rate of absorption of atmospheric CO_2, simulations were performed for all 3713 columns with application rates of 100, 200, 400 gm m^{-2} a^{-1} and so on, up to 1200 gm m^{-2} a^{-1}. The effectiveness of each additional increment in the $CaCO_3$ application rate was computed for each column (giving a total of $7 \times 3713 = 25{,}991$ effectiveness values), then the incremental additions were sorted in order of decreasing effectiveness, beginning with the column increment combination that was most effective in absorbing CO_2. This was done separately for absorption rates 50, 100, and 200 years after addition of limestone powder begins. Figure 7 shows the variation in the rate of absorption with rate of $CaCO_3$ addition when the results are sorted this way, along with the variation of the marginal effectiveness with the rate of $CaCO_3$ addition. As can be seen from Figure 7, after 50 years, there is little further increase in the rate of absorption of CO_2 once the application rate exceeds about 4 billion t $CaCO_3$ a^{-1}. Figure 8 shows the distribution of the application rates in different grid cells for a total application rate of 4 Gt $CaCO_3$ a^{-1}, with absorption after 50 years maximized. Not surprisingly, most of the grid cells in the North Pacific Ocean north of about 45°N are chosen, as well as along the west coast of

the United States of America and Peru. Scattered cells in the Antarctic Ocean are also chosen, in spite of the deep saturation horizons (around 3000 m deep), because of the large upwelling velocities (up to several 100 m a^{-1}) in these regions. Table 4 gives the numbers of columns selected in various application rate/upwelling time bins for the distribution of $CaCO_3$ addition that gives the maximum rate of absorption of CO_2, subject to a total application rate of 4 Gt $CaCO_3$ a^{-1}. Fewer columns with larger average application rate are optimal for a given rate of absorption of atmospheric CO_2 after 50 years than after 100 years. This is because on a 100-year time horizon, columns with upwelling times in the 50–100 year range can contribute to the absorption of CO_2, so more columns can be chosen, but the average application rate will be smaller (given a fixed global application rate). If cells are chosen to maximize the absorption at 50 years, a total area of 14.02 million km^2 receives limestone powder at an average rate of 285.3 gm m^{-2} a^{-1}, whereas maximization of the rate of absorption at 100 years requires applying $CaCO_3$ to an area of 18.56 million km^2 at an average rate of 215.7 gm m^{-2} a^{-1}.

[31] The application of limestone powder at a rate of 4 billion t a^{-1} corresponds to a rate of dissolution of $CaCO_3$ of 0.48 Gt C a^{-1}. By comparison, *Lerman and MacKenzie* [2005] estimate the global rate of production of $CaCO_3$ in the oceans to be 0.64–1.13 Gt C a^{-1} and the global rate of dissolution below the saturation horizon to be 0.25–0.75 Gt C a^{-1}. Thus the dissolution flux considered here is comparable to the natural dissolution flux.

3.4. Analysis of the Effect of Global-Scale Interactions

[32] The preceding results assume that the atmospheric CO_2 concentration is unaffected by the absorption of CO_2 from the atmosphere. This is a valid assumption if addition of limestone powder is done on a small scale. The ocean mixed layer will then absorb enough CO_2 from the atmosphere
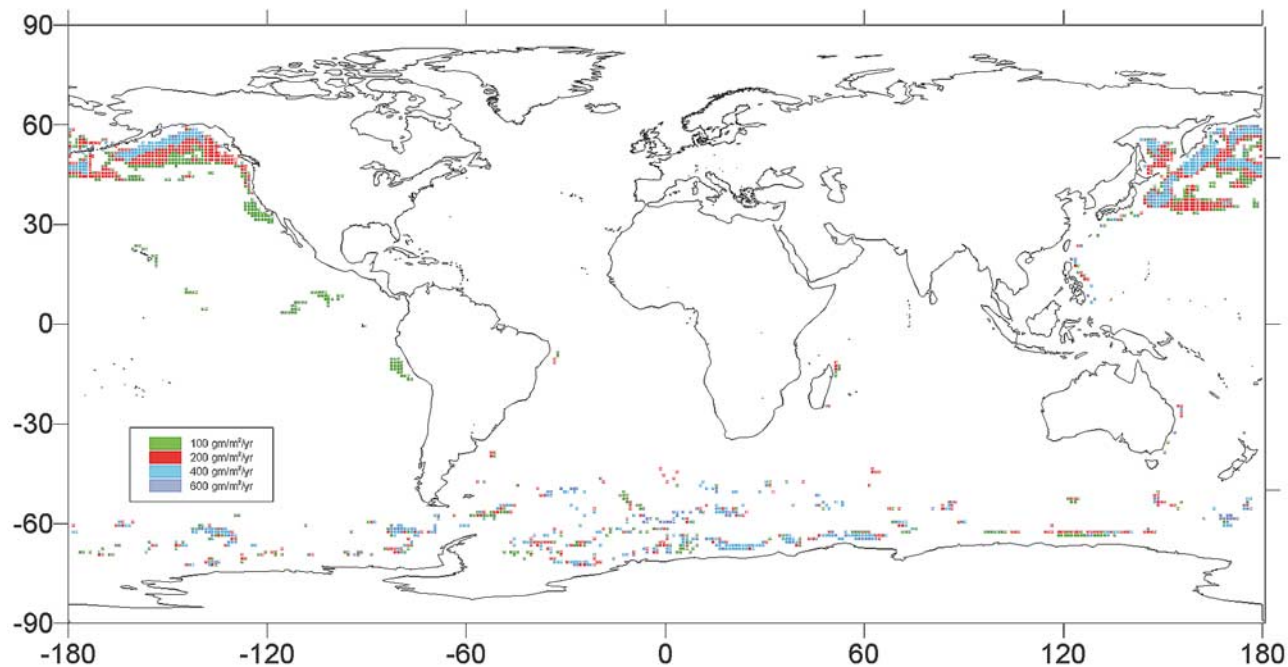
Figure 8. Distribution of the rate of addition of limestone powder (gm m^{-2} a^{-1}) that maximizes the total absorption of CO_2 in year 50, subject to a total application rate of 4 Gt a^{-1}.

to restore the original mixed layer pCO_2 value, but in so doing, the pH and degree of saturation are largely restored to the values prior to addition of limestone powder. In reality, absorption of CO_2 from the atmosphere would reduce the atmospheric pCO_2, so that a smaller increase in mixed layer TDIC is required to restore the original difference between atmospheric and mixed layer pCO_2. This would result in a larger net increase in pH and in the degree of supersaturation. The decrease in atmospheric pCO_2 would cause outgassing of CO_2 in regions not subject to addition of limestone powder, leading to an increase in pH

and in supersaturation in these regions as well, but the outgassing would increase the atmospheric pCO_2 and hence the required increase in TDIC in the regions subject to addition of limestone powder, thereby reducing the pH and supersaturation benefits in those regions.

[33] To analyze this behavior, a simple perturbation analysis can be performed. Two domains will be considered: domain 1, in which limestone powder is added, which produces an initial perturbation in mixed layer pCO_2 designated as $(\Delta pCO_2)_p$ and a subsequent adjustment in pCO_2 designated as $(\Delta pCO_2)_1$, and domain 2, which experiences

Table 4. Number of Columns Chosen From Each Combination of Total Application Rate and Upwelling Time Bin[a]

Application Rate, gm m^{-2} a^{-1}	Upwelling Time, years										
	$0-10$	$10-20$	$20-30$	$30-40$	$40-50$	$50-60$	$60-70$	$70-80$	$80-90$	$90-100$	All Times
Analysis After 50 Years											
100	16	94	144	145	123	0	0	0	0	0	522
200	247	147	53	88	93	0	0	0	0	0	628
400	267	34	107	44	10	0	0	0	0	0	462
600	38	38	28	16	30	0	0	0	0	0	150
800	16	12	2	13	0	0	0	0	0	0	43
1000	5	2	4	5	0	0	0	0	0	0	16
1200	16	7	6	4	0	0	0	0	0	0	33
All rates	605	334	344	315	256	0	0	0	0	0	1854
Analysis After 100 Years											
100	78	150	157	154	118	110	95	118	189	20	1189
200	264	112	76	64	111	121	109	75	0	0	932
400	162	27	45	25	22	25	23	0	0	0	329
600	53	6	16	7	3	2	0	0	0	0	87
800	30	2	7	0	0	0	0	0	0	0	39
1000	4	2	1	0	0	0	0	0	0	0	7
1200	11	5	0	0	0	0	0	0	0	0	16
All Rates	602	304	302	250	254	258	227	193	189	20	2599

[a]Application rate is given as different rows, and upwelling time bin is given as different columns, subject to a total rate of addition of $CaCO_3$ of 4 Gt a^{-1}.

an adjustment $(\Delta pCO_2)_2$. Representing the change in atmospheric pCO_2 as $(\Delta pCO_2)_a$, the required balance equations for domains 1 and 2 are

$$\Delta(pCO_2)_1 - (\Delta pCO_2)_a + (\Delta pCO_2)_p = 0 \qquad (9)$$

$$\Delta(pCO_2)_2 - (\Delta pCO_2)_a = 0, \qquad (10)$$

while conservation of mass requires that

$$\Delta C_1 + \Delta C_2 + \Delta C_a = 0, \qquad (11)$$

where $(\Delta pCO_2)_p$ is computed from the chemistry equations using $\Delta TDIC_p$ and the corresponding alkalinity perturbation, and

$$(\Delta pCO_2)_1 = \Delta TDIC_{adj-1} \frac{\partial pCO_2}{\partial TDIC} \qquad (12)$$

$$(\Delta pCO_2)_2 = \Delta TDIC_{adj-2} \frac{\partial pCO_2}{\partial TDIC} \qquad (13)$$

$$\Delta C_a = \gamma_a (\Delta pCO_2)_a A_a \qquad (14)$$

$$\Delta C_1 = \gamma_{ML} \Delta TDIC_{adj-1} A_1 \qquad (15)$$

$$\Delta C_2 = \gamma_{ML} \Delta TDIC_{adj-2} A_2. \qquad (16)$$

[34] ΔC_a, ΔC_1, and ΔC_2 are the changes in the mass of carbon in the atmosphere, the mixed layer of domain 1, and the mixed layer of domain 2, respectively; A_a, A_1, and A_2 are the corresponding areas, $\gamma_a = 0.004195$ kg m^{-2} ppmv^{-1}, and $\gamma_{ML} = \rho D * MW_C \times 10^{-9} = 0.001232$ kg m^{-2} μmole^{-1} kg^{-1} of TDIC, where ρ is the density of seawater (1027 kg m^{-3}), D is the mixed layer depth (assumed to be 100 m in both domains), and MW_C is the molecular weight of C. From the above, it follows that

$$\Delta TDIC_{adj-1} = -(\Delta pCO_2)_p \left(\frac{\partial pCO_2}{\partial TDIC} + \alpha \right)^{-1} \qquad (17)$$

$$(\Delta pCO_2)_a = -\alpha (\Delta TDIC_{adj-1}) \qquad (18)$$

$$\Delta TDIC_{adj-2} = (\Delta pCO_2)_a \left(\frac{\partial pCO_2}{\partial TDIC} \right)^{-1}, \qquad (19)$$

where

$$\alpha = (\gamma_{ML} A_1) \left(\gamma_a A_a + \left(\frac{\gamma_{ML} A_2}{\partial pCO_2 / \partial TDIC} \right) \right)^{-1}. \qquad (20)$$

[35] The following iterative procedure is used to determine a set of TDIC adjustments such that equations (9) and (10) are satisfied to within 0.001 mbar: $(\Delta pCO_2)_p$ and an

initial partial derivative are computed from the chemistry equations, then initial estimates of $\Delta TDIC_{adj-1}$, $(\Delta pCO_2)_a$, and $\Delta TDIC_{adj-2}$ are made using equations (17), (18), (19), and (20). New values of TDIC for domains 1 and 2 are then computed as

$$TDIC_1^* = TDIC_0 + \Delta TDIC_p + \Delta TDIC_{adj-1}^* \qquad (21)$$

$$TDIC_2^* = TDIC_0 + \Delta TDIC_{adj-2}^*, \qquad (22)$$

respectively, where $TDIC_0$ is the initial TDIC concentration, and $\Delta TDIC^*_{adj-1}$ and $\Delta TDIC^*_{adj-2}$ are either the initial estimates of the required adjustments (for the first calculation) or the sum of all the estimates up to and including the current iteration. $TDIC^*_1$ and $\Delta TDIC^*_2$ are then used in the chemistry equations (along with the corresponding alkalinities) to provide the estimates $(\Delta pCO_2)^*_1$ and $(\Delta pCO_2)^*_a$ of $(\Delta pCO_2)_1$ and $(\Delta pCO_2)_a$, respectively. Because of errors in extrapolating the partial derivative in equations (17), (18), (19), and (20), equation (9) is not satisfied exactly. The residual imbalance is

$$(\Delta pCO_2)^*_p = (\Delta pCO_2)^*_1 - (\Delta pCO_2)^*_a + (\Delta pCO_2)_p, \qquad (23)$$

where $(\Delta pCO_2)^*_a$ is the original estimate of the change in atmospheric pCO_2 (from equation (18)) the first time equation (23) is applied. The residual, $(\Delta pCO_2)^*_p$, is then used in the same way as the original perturbation $((\Delta pCO_2)_p)$ to compute further adjustments in $TDIC_1$, $TDIC_2$, and $(pCO_2)_a$. In the second and later applications of equation (23), $(\Delta pCO_2)^*_a$ is the sum of all estimates of the adjustment in atmospheric pCO_2 up to and including the latest estimate.

[36] Figure 9a shows the variation in $\Delta TDIC_p$, $\Delta TDIC_{adj-1}$, $\Delta TDIC_{adj-2}$, and $(\Delta pCO_2)_a$ when a fixed mass of 2 Gt $CaCO_3$ (0.24 Gt C) is dissolved in the mixed layer of domain 1, as the area of domain 1 ranges from 20% to 100% of the global ocean area. The adjustment in TDIC in domain 1 of course decreases as the fixed amount of $CaCO_3$ is added over a larger domain, but the change in atmospheric pCO_2 and hence the adjustment of TDIC in domain 2 varies only very slightly as the area of domain 1 increases. Figure 9b shows the initial and final changes in pH in domain 1 and the change in pH in domain 2. For the 2 Gt addition of $CaCO_3$, atmospheric pCO_2 decreases by about 0.6 ppmv (0.127 Gt C), while the global mean mixed layer pH increases by about 0.00264, with only a slight dependence (± 0.00006) on the area of domain 1. The separate changes shown for domains 1 and 2 assume that no mixing occurs between these two domains, but this would occur in reality, moving the change in both domains closer to the global mean over time.

3.5. Dissolution of Limestone Powder in Freshwater Flows to the Ocean

[37] Although the maximum feasible rate of addition of dissolved $CaCO_3$ to the mixed layer is computed to be about 0.48 Gt C a^{-1}, by adding limestone powder to the mixed layer and letting it settle into unsaturated waters, it might be possible to dissolve some limestone powder in river water
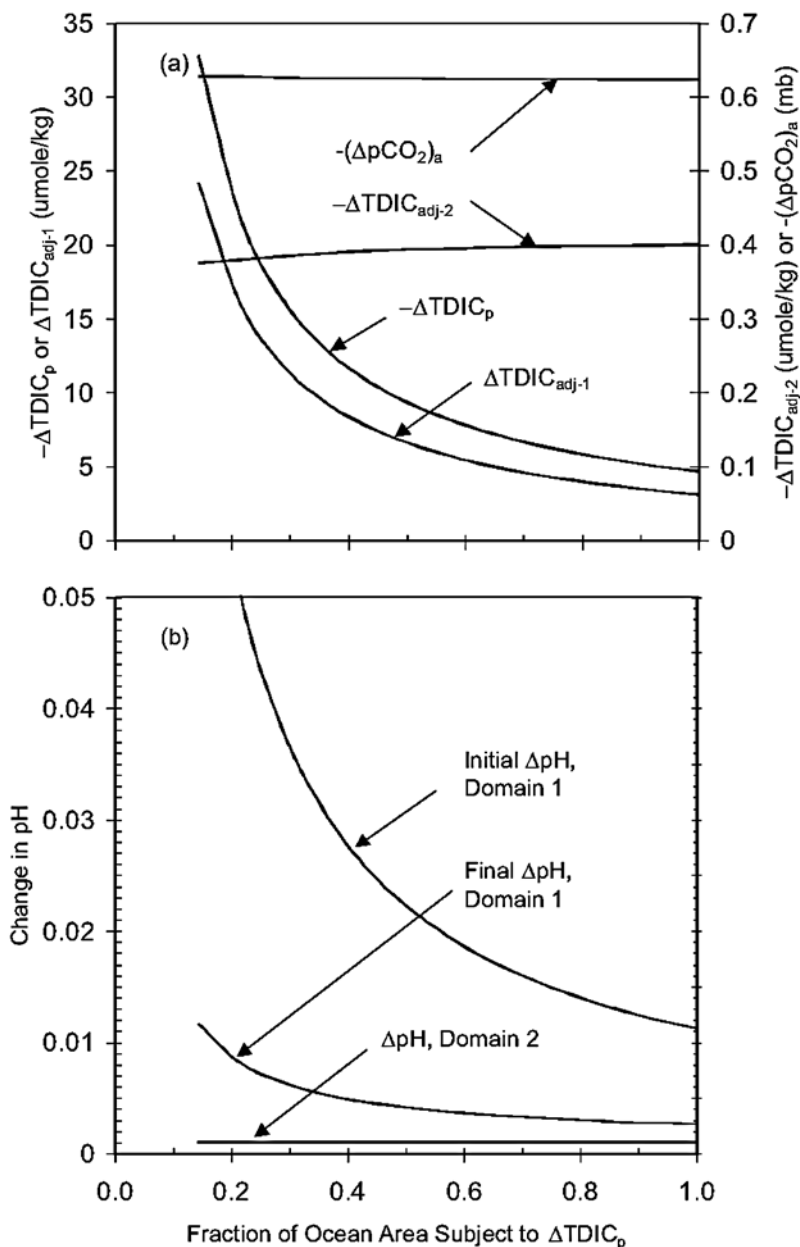
Figure 9. (a) Variation in $\Delta TDIC_p$, $\Delta TDIC_{adj-1}$, $\Delta TDIC_{adj-2}$, and $(\Delta pCO_2)_a$ in response to the addition of 2 Gt $CaCO_3$ as a function of the fraction of the total ocean area over which the $CaCO_3$ is uniformly applied. (b) Change in pH in domains 1 and 2 as a function of the fraction of the total ocean area over which the $CaCO_3$ is uniformly applied.

(which is significantly unsaturated with respect to calcite) just before the river water flows into and mixes with seawater. This would then create an alkalinity perturbation that would be conserved as the river water mixes with ocean water, thereby inducing a perturbation flux of atmospheric CO_2 into the ocean on a timescale of less than 1 year. The potential magnitude of this perturbation flux can be roughly estimated as follows:

[38]   1. The solubility product for calcite at atmospheric pressure is 4.89×10^5 ($\mu mole\ kg^{-1}$)^2.

[39]   2. The concentration of dissolved Ca^{2+} in rivers draining terrain with minimal carbonate rocks (such as the Amazon, Orinoco, and Niger rivers) is on the order of 100 $\mu mole\ kg^{-1}$ (compared to 10,300 $\mu mole\ kg^{-1}$ in seawater with a salinity of 3.5%), as is the initial CO_3^{2-} concentration [see *Depetris and Paolini*, 1991; *Martins and Probst*, 1991].

[40]   3. For these rivers, the dissolution of 600 $\mu mole\ kg^{-1}$ of $CaCO_3$ would bring the water to saturation with respect to calcite.

[41]   4. Assuming a mean annual discharge of 270,000 m^3 s^{-1} for such rivers (about equal to that of the Amazon, Orinoco, and Rio de la Plata rivers alone), that the river water can be brought to within 75% of saturation, and that the ratio of moles absorbed atmospheric CO_2 to moles of $CaCO_3$ added is 0.7, then the rate of addition of dissolved

$CaCO_3$ to the ocean surface water is 0.047 Gt C a^{-1} (0.39 Gt $CaCO_3$ a^{-1}) and the rate of absorption of atmospheric CO_2 from the atmosphere would be 0.033 Gt C a^{-1} (0.12 Gt CO_2 a^{-1}).

[42] 5. For other rivers, where the initial Ca^{2+} and CO_3^{2-} concentrations are typically 700 and 100 μmole kg^{-1}, respectively [see *Telang et al.*, 1991; *Subramanian and Ittekkot*, 1991], the dissolution of only 360 μmole kg^{-1} of $CaCO_3$ would bring the water to saturation with respect of calcite.

[43] 6. If 360 μmole kg^{-1} × 0.75 of $CaCO_3$ were to be dissolved in a river flow of 300,000 m^3 s^{-1} (the total average discharge of the 20 top rivers in terms of discharge is 560,000 m^3 s^{-1}), the rate of dissolution of $CaCO_2$ would be 0.031 Gt C a^{-1}, and the rate of absorption of atmospheric CO_2 would be 0.021 Gt C a^{-1}, bringing the total dissolution to 0.078 Gt C a^{-1} and the total rate of absorption of atmospheric CO_2 to 0.054 Gt C a^{-1} (0.198 Gt CO_2 a^{-1}). This represents a moderate augmentation of the rates of absorption shown in Figure 7.

[44] If Greenland (in a worst case scenario) contributes a sea level rise of 1 m 100 a^{-1}, this would amount to an annual freshwater flux of about 3.6 × 10^{16} kg a^{-1} (twice that of the 20 largest rivers), probably with very low Ca^{2+} and CO_3^{2-} concentrations, although much of the discharge might occur in the form of ice streams rather than as meltwater. Although a goal of climate policy should be to avoid conditions that precipitate rapid melting of the Greenland ice cap, the occurrence of such melting could create conditions favorable to the drawdown of atmospheric CO_2 by adding $CaCO_3$ to the ocean, thereby (in combination with other drastic measures) possibly stabilizing the shrinkage of the ice sheet before an irreversible total collapse is initiated (particularly if several 100 years of sustained warm conditions are needed to provoke complete collapse).

[45] Thus it is concluded that it is unlikely that dissolved $CaCO_3$ could be added to the ocean mixed layer at a rate significantly greater than about 0.56 Gt C a^{-1}, with the bulk of the achievable rate occurring through dissolution of $CaCO_3$ at depth and its subsequent upwelling.

4. Climate-Carbon Cycle Model Simulations

[46] The above results suggest that ground $CaCO_3$ could be effectively applied at a rate of 4 billion t a^{-1} (0.48 Gt C a^{-1}), producing an eventual rate of absorption of CO_2 of about 0.27 Gt C a^{-1} (1 billion t CO_2 a^{-1}).

[47] Here the low-resolution climate-carbon cycle model of *Harvey and Huang* [2001] and *Harvey* [2001] is used to provide a preliminary estimate of the integrated effect of adding ground limestone to ocean. The model used here divides the ocean into a Northern Hemisphere polar downwelling region, a Southern Hemisphere polar upwelling region (which together account for 10% of the ocean area), and the balance of the ocean, where weak upwelling occurs. The ocean component of the model contains the carbonate chemistry of *Peng et al.* [1987]. In light of the results in section 3.3, the effect of adding limestone powder, its dissolution at depth, and subsequent upwelling of the dissolution products can be represented by adding TDIC to the nonpolar mixed layer by an amount that grows from zero in 2020 to 0.48 Gt C a^{-1} in 2120, a rate which is then sustained until the end of the simulation (in 2500). This amounts to the addition of 1.8 μmole kg^{-1} a^{-1} when applied to the entire nonpolar mixed layer, accompanied by a perturbation in TALK that is twice as large. As shown in section 3.4, there is very little difference in the absorption of atmospheric CO_2 if dissolved $CaCO_3$ is applied to a small portion of the mixed layer, or applied uniformly to most of the mixed layer, so applying the $CaCO_3$ to the entire nonpolar mixed layer (as required in the present model) is a valid procedure.

[48] The model is supplied with a scenario of anthropogenic CO_2 emissions. The model computes the absorption of CO_2 by the terrestrial biosphere and oceans; the CO_2 that is not absorbed accumulates in the atmosphere and, along with the buildup of other greenhouse gases, leads to a change in climate which then alters the subsequent absorption of CO_2 by both the terrestrial biosphere and the oceans. Two greenhouse gas (GHG) emission scenarios are considered, one (scenario 1) in which global CO_2 emissions grow to 17.5 Gt C a^{-1} in 2100 and then decline by 1% a^{-1} and another (scenario 2) in which emissions reach 7.5 Gt C a^{-1} by 2010, return to the 2010 level by 2020, and continue down to zero by 2100. This might be achieved in part through capture and sequestration of fossil fuel CO_2 in terrestrial rock strata. Stringent reductions in the emissions of other GHGs and in ozone precursors are also assumed in scenario 2. Three variants of scenario 2 are considered: one in which dissolved limestone is added to the mixed layer at a rate that ramps up to 0.48 Gt C a^{-1} between 2020 and 2120; one in which negative emissions of 1 Gt C a^{-1} are achieved through some combination of sequestration of bioenergy carbon underground and buildup of soil carbon (*Metting et al.* [2001] believe that 0.5–0.8 Gt C a^{-1} could be realistically sequestered worldwide in the soils of biomass cropland while harvesting biomass crops for energy use.), with the rate of sequestration ramping up to 1 Gt C a^{-1} over the period 2020–2050; and one in which dissolved limestone is added at a rate (by 2120) of 1 Gt C a^{-1} (for comparison with the previous case).

[49] Figure 10 shows the resulting variation in global mean temperature and atmospheric CO_2 for all five cases (assuming a climate sensitivity of 3 K for a CO_2 doubling), while Figure 11 shows the variation in ocean mixed layer supersaturation with respect to calcite and pH. The salient observations from these figures are (1) under scenario 1, catastrophic changes in ocean chemistry (calcite supersaturation dropping from 486% to 205% and pH dropping from 8.31 to 7.78) and in climate (7 K global mean warming) occur; (2) the most important factor by far in reducing these impacts is to phase out all fossil fuel CO_2 emissions by the end of this century (supersaturation decreases to 368%, and pH decreases to 8.12); (3) addition of dissolved limestone at the computed maximum feasible rate of 0.48 Gt C a^{-1} allows the supersaturation to recover by about 20% by 2200 (from 368% to 388%) and by 40% by 2500, compared to scenario 2 without addition of $CaCO_3$, while pH recovers by 0.06 by 2200 and by 0.12 by 2500; (4) adding dissolved limestone at a rate of 0.48 Gt C a^{-1} has an effect on mixed layer supersaturation comparable to that of sequestering CO_2 underground and/or in soils at a total rate of 1.0 Gt C a^{-1}, the latter because of the outgassing of CO_2 from the ocean as CO_2 is sequestered; (5) adding dissolved limestone
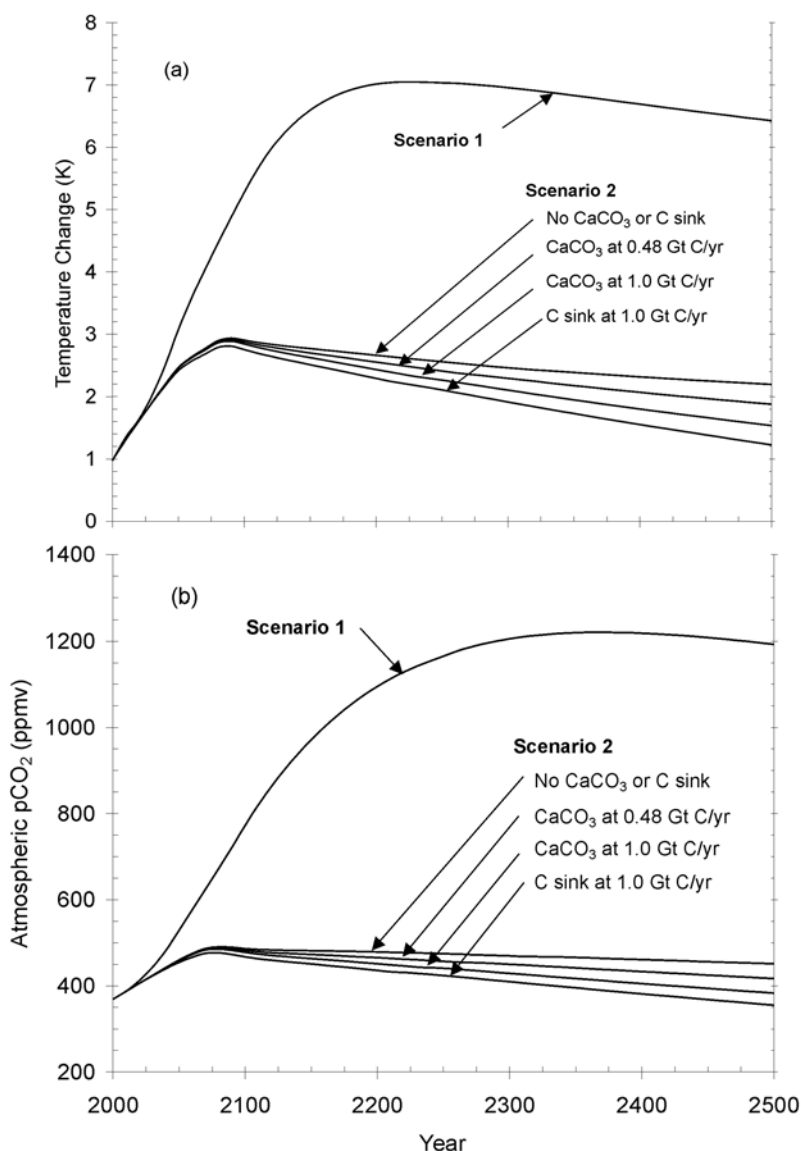
Figure 10. Change in (a) atmospheric temperature and (b) CO_2 concentration for fossil fuel emissions scenario 1 and for scenario 2 with or without addition of $CaCO_3$ powder or terrestrial sequestration of CO_2.

at a rate of 1.0 Gt C a^{-1} has an effect on mixed layer pH comparable to that of sequestering CO_2 underground and/or in soils at a total rate of 1.0 Gt C a^{-1}; and (6) adding dissolved limestone at a rate of 1.0 Gt C a^{-1} has only about three−quarters the effect on atmospheric CO_2 and temperature as sequestering CO_2 at a rate of 1.0 Gt C a^{-1}, this being due to the molar ratio (M_R, equation (8)) being about 0.75.

[50] Perhaps the most surprising result is that building up soil carbon can be as effective in restoring mixed layer pH as adding the some amount of carbon to the ocean in the form of limestone powder, even in the long run after the added limestone powder has had time to dissolve at depth and upwell back to the surface. This is because the effect on ocean pH of dissolving limestone powder is the net result of the direct effect of adding alkalinity, largely offset by the absorption of additional CO_2 from the atmosphere over

time. The sequestration of carbon underground or in soils, on the other hand, induces a direct withdrawal of CO_2 from the ocean. Sequestration of carbon in soils or in geological reservoirs, on the other hand, is only about 50% as effective in restoring the supersaturation of surface waters as adding the same amount of carbon as $CaCO_3$ but is about 30% more effective in reducing the atmospheric CO_2 concentration.

5. Other Considerations

5.1. Magnitude and Cost of the Operation

[51] The current global fossil fuel emission due to the use of coal is about 3 Gt C a^{-1} but is projected to grow to 15−25 Gt C a^{-1} by 2100 in many business-as-usual scenarios. This corresponds to mining coal (which is about 70% C by weight on average) at a rate of about 20−30 Gt a^{-1}. The rate of limestone mining needed to supply 0.48 Gt C a^{-1} is small in comparison, 4 Gt a^{-1}. The amount of crushed stone used
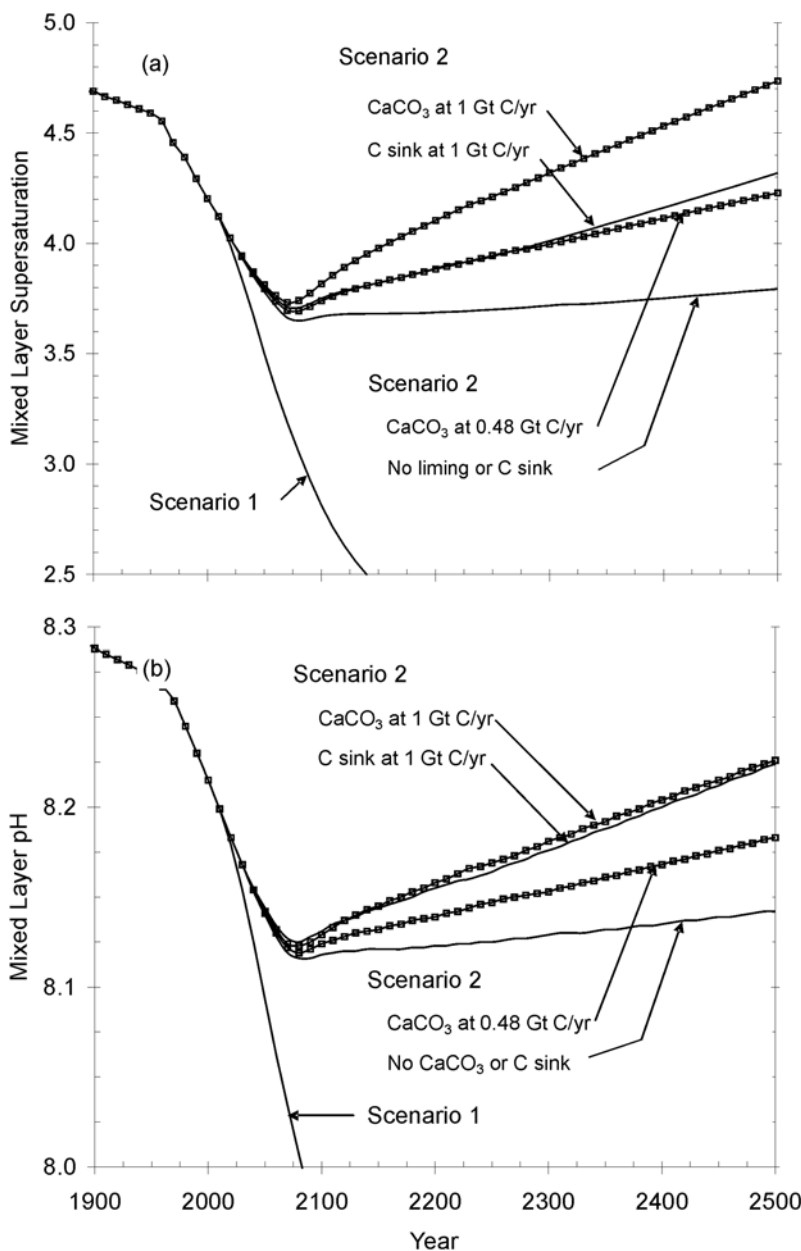
Figure 11. Change in (a) mixed layer supersaturation and (b) mixed layer pH for fossil fuel emissions scenario 1 and for scenario 2 with or without addition of $CaCO_3$ powder or terrestrial sequestration of CO_2.

in the United States per year is about 1.1 Gt, of which two thirds (0.731 Gt) is limestone (see http://minerals.usgs.gov/minerals/pubs/commodity/stone_crushed/stat/tbl2.txt). Carbonate minerals compose about 20% of all Phanerozoic sedimentary rocks, so there is no shortage of suitable rocks. Nevertheless, an enormous infrastructure involving rail transport, processing facilities, port facilities, ships, and possible dedicated wind farms to supply electricity for grinding would have to be built up at the same time that the coal industry is phased out and replaced with various carbon-free energy sources. Also, there will be environmental impacts on land associated with the mining of additional large quantities of limestone that would need to be traded off against the global-scale benefits of adding limestone powder to the ocean.

[52] The market cost of limestone in the United States is around \$5 t^{-1} [*Rau et al.*, 2007]. This includes the cost of mining, crushing (to a size suitable for construction materials), and transportation. *Rau et al.* [2007] indicate transportation costs of \$0.034 $t\text{-}km^{-1}$, \$0.010 $t\text{-}km^{-1}$, and \$0.003 $t\text{-}km^{-1}$ for transport by train, barge, and freighter, respectively. If \$5 $t\text{-}km^{-1}$ is the cost for delivery to the coast, and if the average transport distance by ocean freighter is 1000 km, then the average cost would be \$8 t^{-1}, plus additional costs of \$1−3 t^{-1} for grinding the limestone to a powder (see below). At an application rate of 4 Gt a^{-1}, the total cost would likely be on the order of \$40−45 billion a^{-1}.

5.2. Energy Required to Grind Limestone to Powder and Deliver It to Port

[53] Crushed limestone is currently used as an additive to agricultural soils in order to counter the acidification that would otherwise occur through repeated application of nitrogen fertilizers. *West and Marland* [2002] indicate an energy use for transportation by train of 0.7 MJ t−km^{-1}, but *International Maritime Organization (IMO)* [2000a] obtained (using a simulation model) a rail energy use of only 0.27 MJ t−km^{-1} for a transport distance of 2000 km and 0.52 MJ t−km^{-1} for a transport distance of 200 km. For transport over an average distance of 1000 km from the mining site to coastal ports, energy use of 0.45 MJ t−km^{-1}, and a transport fuel emission factor of 22 kg C GJ^{-1} (including refinery emissions), the CO_2 emission would be 0.0088 t C/t $CaCO_3$. As for the energy used to grind the limestone, this can be computed as

$$E_g = 0.01 W_i \left(\frac{1}{\sqrt{d_1}} - \frac{1}{\sqrt{d_0}} \right), \qquad (24)$$

where d_0 and d_1 are the initial and final particle diameters and W_i is the working index which, for limestone, has a value of 11.6 kWh t^{-1} (1 kWh = 3.6 × 10^6 J) [*Huijgen et al.*, 2006]. For d_0 and d_1, equal to 0.1 m and 80 μm, respectively, E_g = 13.9 kWh t^{-1}. The energy use predicted by equation (24) is only indicative of the actual energy use, being dependent on local materials and equipment efficiencies. *Kojima et al.* [1997], for example, indicates that crushing wollastonite ($CaSiO_3$, having W_i = 14 kWh t^{-1}) from 200 mm to 75 μm requires 43 kWh t^{-1}, compared to 17.6 kWh t^{-1} expected using equation (24). Adopting 15−45 kWh t^{-1} as the crushing electricity use for limestone and assuming the electricity to be generated from coal at 40% efficiency, the CO_2 emission would be 0.0031−0.0093 t C/t $CaCO_3$. At \$0.06 kWh^{-1}, the cost of grinding would be \$0.90−2.70 t^{-1} plus amortization of the cost of the grinding facilities. The total emission would be 0.012−0.018 t C/t $CaCO_3$, plus additional emissions for transport and dispersal of the limestone powder by ship (discussed below). By comparison, the average rate of absorption of CO_2 (given the average effectiveness of 0.25 inferred from Figure 7 when $CaCO_3$ is applied at a rate of 4 Gt a^{-1}) will be about 0.068 t C/t $CaCO_3$. Clearly, CO_2 emissions associated with supplying the limestone powder would offset a significant fraction of the CO_2 absorbed by the oceans if the electricity for grinding is supplied by coal and the limestone is not mined near the coast.

[54] However, fossil fuels as a source of electricity and transportation energy will need to be eliminated within this century if CO_2 is to peak at no more than 450−500 ppmv and then be drawn down through sequestration of bioenergy carbon. The supply of limestone powder then becomes an additional energy demand that will need to be met through renewable energy sources. However, given that limestone crushing could be a dispatchable energy load, it could improve the economics of large-scale implementation of intermittent renewable energy sources (such as wind), in that the renewable energy sources could be oversized relative to the other energy loads (in order to improve the overall fraction of the energy load supplied), and when excess energy is available, this energy could be used for grinding limestone rather than discarded.

[55] During the transition to a carbon-free energy system, the renewable energy sources used by the grinding and other operations could have been used instead to accelerate the reduction in the use of fossil fuels and in associated greenhouse gas emissions. Thus careful optimization in the timing of limestone operations relative to other measures to reduce net GHG emissions will be needed, particularly given the long lag (up to 100 years) between the beginning of limestone addition and an impact on the oceanic uptake of CO_2. On the other hand, the limestone operation is not solely a measure to reduce atmospheric pCO_2 but also serves to partly reverse deleterious changes in ocean chemistry.

5.3. Logistics of and Energy Use Associated With Dispersal by Ship

[56] The largest oil supertankers carry about 650,000 t of oil with a top speed of 30 km h^{-1}, and as of the year 2000, there was a world fleet of 6878 oil tankers with an average capacity of 39,300 t and a total capacity of 270.3 million t [*IMO*, 2000a]. However, large ships would be used only to transport limestone powder to a number of central points, at which point it would be transferred to much smaller ships for dispersal. To determine how many ships would be needed, we need to first estimate the dose of powder that could be applied as the ships traverse a given sector. Suppose that the limestone powder were applied at a rate of 200 gm m^{-2} a^{-1}. This is equal to 2 moles m^{-2} which, if dissolved over a depth 1000 m, would increase the CO_3^{2-} concentration by 2 μmole kg^{-1}, which is small compared to the typical departure from saturation (5−15 μmole kg^{-1}) in the first 1000 m below the saturation horizon. Thus it might be possible to apply the annual limestone dose in one application. However, I shall cautiously assume applications of only 10 and 100 gm m^{-2} at a time, which would require 2−20 traverses across a given region per year. If powder can be sprayed from the ship uniformly over a path 100 m wide, and the ship travels at 30 km h^{-1}, powder would be applied at a rate of 30 and 300 t h^{-1} for application doses of 10 and 100 gm m^{-2}, respectively.

[57] Suppose that 2500-t local delivery ships apply limestone powder at a dose of 100 gm m^{-2}. Then, 8.3 h would be required for dispersing the load of powder. If there is a 650,000-t supply ship in each of the 2500 1° × 1° grid cells (or rather, in an equivalent rectangular area) that would receive limestone powder in the 4 Gt a^{-1} scenario, the greatest distance that the local ship would have to travel for resupply would be about 50 km (given that routes could be designed so that a dispersal ship finishes as close to the supply ship on average as possible), so it is reasonable to assume a total time of no more than 14 h per load, thereby permitting at least 625 loads per year. Then, 2560 such ships would be required to deliver 4 Gt of $CaCO_3$ a^{-1}, and 250 loads (3500 h) would be required to empty the 650,000-t central ship, so there would be time for two deliveries per year (recall that the distance traveled by the central ships would not be large, as limestone would be largely applied to the North Pacific Ocean from nearby specially built ports). Thus 3000 central ships would be needed. However, if the central ships each serve four 2500-t local ships covering

Table 5. Derivation of Energy Use by, Peak and Average Power Requirements of, and Peak and Average Photovoltaic (PV) Power Available to Ships of Various Sizes That Could Be Used for Dispersing Limestone Powder Over the Ocean[a]

	Ship Capacity, t					
	2500	2500	25,000	25,000	250,000	250,000
Rate of application, gm m^{-2}	10	100	10	100	10	100
Rate of application, t km^{-1}	1	10	1	10	1	10
Distance travelled, km	2500	250	25,000	2500	250,000	25,000
Hours required	83	8.3	833	83	8333	833
Energy intensity, MJ t$-$km^{-1}	0.23	0.23	0.19	0.19	0.064	0.064
Energy use, GJ t applied^{-1}	0.575	0.0575	4.75	0.475	16	1.6
Carbon emission, t CaCO$_3$ applied^{-1}	0.01265	0.001265	0.1045	0.01045	0.352	0.0352
Initial C emission, C absorbed^{-1}	0.1326	0.0133	1.0958	0.1096	3.6910	0.3691
Final C emission, C absorbed^{-1}	0.5158	0.0516	4.2613	0.4261	14.3538	1.4354
Average power required, MW	4.8	4.8	39.6	39.6	133.3	133.3
Volume of cargo, m^3	1000	1000	10,000	10,000	100,000	100,000
Height of cargo area, m	5	5	10	10	20	20
Peak PV power, MW	30	30	150	150	750	750
Daily average PV power, MW	3.6	3.6	18	18	90	90

[a] See text for specific assumptions.

somewhat less than a 2° × 2° grid cell, and if the average time per round trip by the local ships increases to 16 h (to allow for the greater average return distance to the central ship), the central ship could be unloaded in 1000 h. This would permit close to eight deliveries per year rather than two, reducing the number of such ships to about 750 from 3000. The number of 2500-t ships required would increase from 2560 to 2925 (not allowing for downtime due to maintenance and the resulting need for backup ships), which is small compared to the total world fleet of 43,325 ships given by *IMO* [2000a, Figures 3, 4, 5, 6, and 7]. If more local ships are supplied by a single central ship, the required number of large central ships could be reduced further.

[58] Table 5 gives the derivation of the average energy required by ships per tonne of limestone applied to the ocean (this is in addition to the energy given above for mining, grinding, and transport by train to ports). The assumptions are as follows: Limestone powder is applied at a density of 10 gm m^{-2} or 100 gm m^{-2} along the path of a ship; the width of application zone is 100 m; and the energy use for transport by ship is 0.23, 0.19, and 0.064 MJ t$-$km^{-1} for 2500-t, 25,000-t, and 250,000-t ships, respectively. The energy intensities are taken from work by *IMO* [2000b, Table 4.9] but have been scaled to a travel speed of 30 km, assuming the energy intensity to vary with the square of the speed. *IMO* [2000b, Figures 4, 5, 6, 7, 8, 9, and 10] indicated that the energy intensity at half of full load is approximately twice that at full load, which implies that the energy use per kilometer is independent of the load (at least between loads of 50 and 100%). Energy use per tonne of applied limestone is thus computed using t-km given by the initial load times the distance required to disperse all of the limestone powder in a given load. The energy requirement ranges from 0.0575 GJ t^{-1} for 2500-t ships and a 100 gm m^{-2} application per traverse to 16.0 GJ t^{-1} for 250,000-t ships and a 10 gm m^{-2} application per traverse. There are significant energy savings in using small ships to apply the limestone because small ships have the smallest average payload (so the total t-km of transport is smallest). Energy requirements would therefore be substantially re-

duced if large ships are positioned in the center of a given area that would be serviced by several smaller ships.

[59] Additional energy would be required to project the limestone powder over a 100-m wide swath. The greatest distance projected would be 50 m which, neglecting air resistance, would require a velocity of 26.9 m s^{-1} inclined at an angle of 21.8° from the horizontal. This is a kinetic energy requirement of 0.36 MJ t^{-1}, which is negligibly small compared to the energy required to propel the ship per tonne of applied limestone powder.

[60] Also shown in Table 5 is the CO$_2$ emission (t C t^{-1} CaCO$_3$) if the ship energy is supplied by diesel fuel (assuming an emission factor of 0.022 t C GJ^{-1}, which includes typical upstream emissions associated with refining of crude petroleum). The emission ranges from 0.0133 t C/t CaCO$_3$ to 0.352 t C/t CaCO$_3$. By comparison, the marginal effectiveness of the limestone powder (i.e., the incremental absorption of CO$_2$ from the atmosphere over incremental limestone addition) ranges from 0.0954 t C/t CaCO$_3$ for the first increment of CaCO$_3$ added to 0.0245 t C/t CaCO$_3$ for the final increment added when the total reaches 4 Gt a^{-1} (these are the marginal effectivenesses in t CO$_2$/t CaCO$_3$, given in Figure 7, divided by 3.67 to give t C/t CaCO$_3$). The next two rows of Table 5 give the ratio of CO$_2$ emitted to CO$_2$ absorbed for the initial and final marginal effectivenesses. The ratio for the final increment is only 0.0516 for 2500-t ships and a 100 gm m^{-2} dose and 0.426 for 25,000-t ships and a 100 gm m^{-2} dose but is larger than 1.0 for 250,000-t ships.

[61] The final rows of Table 5 give the average power required to propel the ship and the average power that could be generated if photovoltaic (PV) modules at 15% conversion efficiency cover the deck of the ship (assuming an average solar irradiance of 120 W m^{-2} and cargo hold heights of 5, 10, and 20 m for the 2500-t, 25,000-t, and 250,000-t ships, respectively). The average available solar power exceeds or roughly equals the average power requirement for ships of all sizes. Excess peak solar energy could be stored in a battery sized to store only a few hours of excess energy. The DC output of PV modules could be used to directly power a DC motor (thereby avoiding

DC-AC conversion losses), with assistance from a diesel (or biodiesel) engine only as needed (as in hybrid gasoline-electric cars).

5.4. Ecological Impacts

[62] Once the added $CaCO_3$ powder to the ocean surface layer has dissolved, it would likely have no impact other than to neutralize the increase in oceanic acidity and the decrease in $CaCO_3$ supersaturation due to the absorption of anthropogenic CO_2 by the oceans. There could be some impact from impurities in the $CaCO_3$, but these impurities would be beneficial if they act as nutrients. However, it is possible but not likely that large zooplankton would not distinguish between food particles and limestone particles and would thereby ingest some of the falling limestone particles. This would have adverse effects on the zooplankton and would also result in the particles being repackaged in feces, causing faster sinking and slower dissolution. However, as noted in section 5.3, the limestone powder could be applied in only a few doses per year, and with a settling velocity on the order of 600 m d^{-1}, would spend only a few hours per year in the photic zone or in layers of comparable thickness.

[63] The addition of limestone powder would likely increase the albedo of the ocean surface, while slightly decreasing the penetration of solar radiation into the mixed layer. The former would have a slight cooling effect and so would be beneficial in the context of unwanted global warming, while the latter could reduce the strength of the biological pump. Occasional coccolithophore blooms have been observed to reflect 10–20% of the incident solar radiation near the wavelengths of peak irradiance [*Balch et al.*, 1996a]. However, given only a few applications of limestone per year and a settling velocity on the order of 600 m d^{-1}, the fraction of the year subject to any albedo and solar radiation effects would be very small. Also, light scattering per unit mass by calcite is largest for particle sizes of 1–2 μm and falls sharply with increasing size [*Balch et al.*, 1996b].

5.5. Impacts of Marine Biota on the Effectiveness of the Proposed Scheme

[64] The only other proposal known to the author to induce greater absorption of atmospheric CO_2 by the ocean is the idea of adding iron to the ocean. This idea is based on the observation that in many parts of the ocean, iron is a limiting nutrient, so addition of iron would stimulate marine photosynthesis, leading to an increased downward flux of organic matter from the surface layer to the deep ocean. Unfortunately, a number of studies have shown that this does not lead to a long-term increase in the absorption of atmospheric CO_2 by the ocean because much of the organic matter exported from the surface layer dissolves and diffuses back into the surface layer [*Buesseler et al.*, 2004; *Zeebe and Archer*, 2005]. The beauty of the scheme proposed here is that it does not rely on the response of the marine biota. Instead, the absorption of atmospheric CO_2 in response to adding limestone powder occurs in response to inorganic (and well-established) chemical reactions.

[65] The proposed scheme could nevertheless be affected by biological processes. One possibility is that dissolved organic carbon in the seawater could cause limestone particles to aggregate together. This would increase the settling velocity and, more importantly, reduce the volumetric rate of dissolution. Thus less dissolved carbonate would be made available to initially neutralize oceanic acidity and to take up additional atmospheric CO_2. The aggregation rate would depend on the size, number, and spread in the settling velocities of the powder particles (differential settling would allow them to collide and coalesce if dissolved organic carbon has a chance to adhere to the particles first). *Passow and De La Rocha* [2006] performed experiments in tanks to test the ability of organic materials to cause aggregation of calcium carbonate particles. They found that suspended $CaCO_3$ minerals are efficiently scavenged by and incorporated into organic aggregates. However, they only used particles with a fall velocity of <1.0 m d^{-1}, which implies a diameter of roughly 3 μm. Aggregation might be more difficult with the 80−μm size particles considered here than with the much smaller particles commonly found in ocean water, but this question needs further investigation through field experiments.

[66] It is likely that carbon cycle feedbacks involving the marine biota would slightly weaken the effect of adding limestone powder to the ocean. In particular, the restoration of the surface layer calcium carbonate supersaturation back to the preindustrial level will likely cause greater growth of calcareous plankton compared to the nonmitigation scenario (this is one of the intended effects), but this is the opposite to the dissolution of $CaCO_3$ and so will result in a smaller net absorption of atmospheric CO_2. Assessment of the magnitude of this feedback requires simulations with detailed models of marine ecosystems, calibrated with experimental data on the effect of different CO_2 concentrations on the relative growth rates of calcareous and noncalcareous organisms.

5.6. Precipitation of Calcite in the Supersaturated Zone

[67] There is the possibility that the presence of limestone particles in the supersaturated upper part of the water column could induce precipitation of $CaCO_3$ onto the particles. This would have opposite to the intended effect on surface water pH, carbonate supersaturation, and absorption of atmospheric CO_2. This phenomenon has been observed in the "whitings" that periodically appear on the Great Bahama Bank [*Morse et al.*, 2003]. The whitings consist of carbonate sediments that are periodically lifted into suspension by turbulence. The whiting particles typically are on the order of 1 μm in size, which corresponds to a surface area of about 0.95 m^2 gm^{-1}. The 80−μm particles considered here, in contrast, would have a surface area of only 0.027 m^2 gm^{-1} (35 times less). In as much as the rate of precipitation depends on the surface area (and time) available, precipitation is not likely to be a significant factor.

6. Concluding Comments

[68] The calculations presented here serve to illustrate the enormity of the task of even partially reversing the acidification of the oceans that is yet to occur under even the most optimistic scenarios concerning reductions in CO_2 emissions. The task is not only enormous but would need to continue for several 100 years. These calculations also underline the fact that in the absence of stringent reductions

in CO_2 emissions, efforts to reduce adverse impacts on ocean chemistry will be ineffective.

[69] The single largest factor in limiting the acidification of the ocean is to switch from a trajectory of increasing CO_2 emissions to one in which emissions have dropped to zero by the end of this century (mean mixed layer pH drops from a preindustrial value 8.31 to 8.12 if emissions are zero by 2100 instead of dropping to 7.78 if emissions peak at 17.5 Gt C a^{-1} in 2100). If anthropogenic CO_2 emissions have been reduced to zero by 2100, then application of limestone at a rate of 4 Gt a^{-1} (0.48 Gt C a^{-1}) beginning in 2020 serves to restore about 20% of the difference between the minimum pH and preindustrial pH by 2200 and restores about 40% of the difference by 2500, with the same benefits for the degree of supersaturation with respect to calcite.

[70] Compared to sequestering 0.5 Gt C a^{-1} in soils or in geological strata, adding 0.5 Gt C a^{-1} of dissolved $CaCO_3$ to the mixed layer (by adding 4 Gt a^{-1} of limestone powder) has (1) about twice the effect of mixed layer supersaturation, (2) about the same effect on mixed layer pH, and (3) about three-quarters the effect on atmospheric pCO_2 and temperature change.

[71] However, the impacts of sequestering CO_2 are immediate, whereas the benefits of adding limestone powder are delayed by up to 100 years. Nevertheless, the buildup of biomass carbon on land or the underground sequestration of bioenergy carbon are alternative or complementary strategies to adding limestone powder to the ocean for restoring the pH and supersaturation of the ocean mixed layer (and atmospheric CO_2 concentration) to values close to those at present.

[72] It has been argued here that both potential adverse effects of adding limestone powder to the mixed layer on the marine biota and inhibition of the desired effect by the marine biota are likely to be very small. Nevertheless, there are many uncertainties concerning the interaction between limestone powder and the marine biota, and there could be surprises in the outcome.

[73] The results presented here have been obtained through a series of column calculations and using a simple low-resolution model. An important next step will be to assess the impact of adding limestone powder to specific regions of the ocean using a high-resolution ocean general circulation model with the required chemistry submodules and with embedded ecosystem models to assess feedbacks between the marine biota and mixed chemistry. If this idea is to be pursued further, field experiments will be required to determine the settling velocities and rates of dissolution of samples of natural limestone that have been ground to various sizes and to determine possible effects of and impacts on biological processes.

References

Balch, W. M., K. A. Kilpatrick, and C. C. Trees (1996a), The 1991 coccolithopore bloom in the central North Atlantic. 1. Optical properties and factors affecting their distribution, *Limnol. Oceanogr.*, 41, 1669–1683.

Balch, W. M., K. A. Kilpatrick, P. M. Holligan, D. Harbour, and E. Fernandez (1996b), The 1991 coccolithopore bloom in the central North Atlantic. 2. Relating optics to coccolith concentration, *Limnol. Oceanogr.*, 41, 1684–1696.

Broecker, W. S., and T. Takahashi (1978), The relationship between lysocline depth and in situ carbonate ion concentration, *Deep Sea Res.*, 25, 65–95.

Buesseler, K. O., J. E. Andrews, S. M. Pike, and M. A. Charette (2004), The effects of iron fertilization on carbon sequestration in the Southern Ocean, *Science*, 304, 414–417.

Caldeira, K., and G. H. Rau (2000), Accelerating carbonate dissolution to sequester carbon dioxide in the ocean: Geochemical implications, *Geophys. Res. Lett.*, 27, 225–228.

Depetris, P. J., and J. E. Paolini (1991), Biogeochemical aspects of South American rivers: The Paraña and the Orinoco, in *Biogeochemistry of Major World Rivers*, vol. 42, *SCOPE Rep.*, edited by E. T. Degens, S. Kempe, and J. E. Richey, pp.105–125, John Wiley, Chichester, U.K.

Dickson, A. G. (1990), Thermodynamics of the dissociation of boric acid in synthetic seawater from 273.15 to 318.15 K, *Deep Sea Res., Part A*, 37, 755–766.

Dickson, A. G., and F. J. Millero (1987), A comparison of the equilibrium constants for the dissociation of carbonic acid in sea water media, *Deep Sea Res., Part A*, 34, 1733–1743.

Gazeau, F., C. Quiblier, J. M. Jansen, J.-P. Gattuso, J. J. Middelburg, and C. H. R. Heip (2007), Impact of elevated CO_2 on shellfish calcification, *Geophys. Res. Lett.*, 34, L07603, doi:10.1029/2006GL028554.

Hales, B., and S. Emerson (1997), Evidence in support of first-order dissolution kinetics of calcite in seawater, *Earth Planet. Sci. Lett.*, 148, 317–327.

Harvey, L. D. D. (2000), *Global Warming: The Hard Science*, 336 pp., Prentice-Hall, Upper Saddle River, N. J.

Harvey, L. D. D. (2001), A quasi-one-dimensional coupled climate-carbon cycle model 2. The carbon cycle component, *J. Geophys. Res.*, 106, 22,355–22,372.

Harvey, L. D. D., and Z. Huang (2001), A quasi-one-dimensional coupled climate-carbon cycle model: 1. Description and behavior of the climate component, *J. Geophys. Res.*, 106, 22,339–22,353.

Huijgen, W. J. J., G. J. Ruijg, R. N. J. Comans, and G.-J. Witkamp (2006), Energy consumption and net CO_2 sequestration of aqueous mineral carbonation, *Ind. Eng. Chem. Res.*, 45(26), 9184–9194.

Intergovernmental Panel on Climate Change (IPCC) (2005), *Special Report on Carbon Dioxide Capture and Storage*, edited by B. Metz et al., 443 pp., Cambridge Univ. Press, New York.

International Marine Organization (IMO) (2000a), Study of greenhouse gas emissions from ships: Final report to the International Maritime Organization, edited by K. O. Skjølsvik et al., *MT Rep. MT00 A23-038*, London. (Available at http://unfccc.int/files/methods_and_science/emissions_from_intl_transport/application/pdf/imoghgmain.pdf.)

International Marine Organization (IMO) (2000b), Study of greenhouse gas emissions from ships: Appendices, edited by K. O. Skjølsvik et al., *Append. to MT00 A23-038*, London. (Available at http://unfccc.int/files/methods_and_science/emissions_from_intl_transport/application/pdf/imoghgapp.pdf.)

Jin, X., N. Gruber, J. P. Dunne, J. L. Sarmiento, and R. A. Armstrong (2006), Diagnosing the contribution of phytoplankton functional groups to the production and export of particulate organic carbon, $CaCO_3$, and opal from global nutrient and alkalinity distributions, *Global Biogeochem. Cycles*, 20, GB2015, doi:10.1029/2005GB002532.

Key, R. M., A. Kozyr, C. L. Sabine, K. Lee, R. Wanninkhof, J. L. Bullister, R. A. Feely, F. J. Millero, C. Mordy, and T.-H. Peng (2004), A global carbon climatology: Results from Global Data Analysis Project (GLODAP), *Global Biogeochem. Cycles*, 18, GB4031, doi:10.1029/2004GB002247.

Kheshgi, H. S. (1995), Sequestering atmospheric carbon dioxide by increasing ocean alkalinity, *Energy*, 20, 915–922.

Kojima, T., A. Nagamine, N. Ueno, and S. Uemiya (1997), Absorption and fixation of carbon dioxide by rock weathering, *Energy Convers. Manage.*, 38, 461–466.

Lerman, A., and F. T. Mackenzie (2005), CO_2 air-sea exchange due to calcium carbonate and organic matter storage, and its implications for the global carbon cycle, *Aquat. Geochem.*, 11, 345–390.

Martins, O., and J.-L. Probst (1991), Biogeochemistry of major Africa rivers: Carbon and mineral transport, in *Biogeochemistry of Major World Rivers*, vol. 42, *SCOPE Rep.*, edited by E. T. Degens, S. Kempe, and J. E. Richey, pp.127–155, John Wiley, Chichester, U.K.

Metting, F. B., J. L. Smith, J. S. Amthor, and R. C. Isaurralde (2001), Science needs and new technology for increasing soil carbon sequestration, *Clim. Change*, 51, 11–34.

Morse, J. W., and R. S. Arvidson (2002), The dissolution kinetics of major sedimentary carbonate minerals, *Earth Sci. Rev.*, 58, 51–84.

Morse, J. W., D. K. Gledhill, and F. J. Millero (2003), $CaCO_3$ precipitation kinetics in waters from the Great Bahama Bank: Implications for the relationship between bank hydrochemistry and whitings, *Geochim. Cosmochim. Acta*, *67*, 2819–2826.

Orr, J. C., et al. (2005), Anthropogenic ocean acidification over the twenty-first century and its impact on calcifying organisms, *Nature*, *437*, 681–686.

Passow, U., and C. L. De La Rocha (2006), Accumulation of mineral ballast on organic aggregates, *Global Biogeochem. Cycles*, *20*, GB1013, doi:10.1029/2005GB002579.

Peng, T.-H., T. Takahashi, W. S. Broecker, and J. Olafsson (1987), Seasonal variability of carbon dioxide, nutrients and oxygen in the northern North Atlantic surface water: Observations and a model, *Tellus, Ser. B*, *39*, 439–458.

Rau, G. H., and K. Caldeira (1999), Enhanced carbonate dissolution: A means of sequestering waste CO_2 as ocean bicarbonate, *Energy Convers. Manage.*, *40*, 1803–1813.

Rau, G. H., K. G. Knauss, W. H. Langer, and K. Caldeira (2007), Reducing energy-related CO_2 emissions using accelerated weathering of limestone, *Energy*, *32*, 1471–1477.

Raven, J., K. Caldeira, H. Elderfield. O. Hoegh-Guldberg, P. Liss, U. Riebesell, J. Shepherd, C. Turley, and A. Watson (2005), Ocean acidification due to increasing atmospheric carbon dioxide, *Policy Doc. 12/05*, R. Soc., London, 30 Jun.

Riebesell, U., I. Zondervan, B. Rost, P. D. Tortell, R. E. Zeebe, and F. M. M. Morel (2000), Reduced calcification of marine plankton in response to increased atmospheric CO_2, *Nature*, *407*, 364–367.

Ruttimann, J. (2006), Sick seas, *Nature*, *442*, 978–980.

Subramanian, V., and V. Ittekkot (1991), Carbon transport by the Himalayan rivers, in *Biogeochemistry of Major World Rivers*, vol. 42, *SCOPE Rep.*, edited by E. T. Degens, S. Kempe, and J. E. Richey, pp. 157–168, John Wiley, Chichester, U.K.

Takahashi, T., et al. (2008) Climatological mean and decadal change in the surface ocean pCO_2, and the net sea-air CO_2 flux over the global oceans, *Deep Sea Res., Part II*, in press.

Telang, S. A., R. Pocklington, A. S. Naidu, E. A. Romankevich, I. I. Gitelson, and M. I. Gladyshev (1991), Carbon and mineral transport in major North America, Russian Arctic, and Siberian rivers: The St. Lawrence, the Mackenzie, the Yukon, the arctic Alaskan rivers, the arctic basin rivers in the Soviet Union, and the Yemisei, in *Biogeochemistry of Major World Rivers*, vol. 42, *SCOPE Rep.*, edited by E. T. Degens, S. Kempe, and J. E. Richey, pp. 75–104, John Wiley, Chichester, U.K.

West, T. O., and G. Marland (2002), A synthesis of carbon sequestration, carbon emissions, and the net carbon flux in agriculture: Comparing tillage practices in the United States, *Agric. Ecosyst. Environ.*, *91*, 217–232.

Wunsch, C., and P. Heimbach (2000), Practical global oceanic state estimation, *Physica D*, *230*, 197–208, doi:10.1016/j.physd.2006.09.040.

Zeebe, R. E., and D. Archer (2005), Feasibility of ocean fertilization and its impact on future atmospheric CO_2 levels, *Geophys. Res. Lett.*, *32*, L09703, doi:10.1029/2005GL022449.

————————————

L. D. D. Harvey, Department of Geography, University of Toronto, 100 St. George Street, Toronto, Ontario, Canada M5S 3G3. (harvey@geog.utoronto.ca)